UNCLASSIFIED

AD-A285 498

Dist: A

ORT DOCUMENTATION PAGE

1a. Unclassified	1b. RESTRICTIVE MARKINGS N/A
2a. SECURITY CLASSIFICATION AUTHORITY N/A	3. DISTRIBUTION / AVAILABILITY OF REPORT Unlimited A
2b. DECLASSIFICATION / DOWNGRADING SCHEDULE N/A	
4. PERFORMING ORGANIZATION REPORT NUMBER(S) N/A	5. MONITORING ORGANIZATION REPORT NUMBER(S) AFOSR-TR- 94 0625
6a. NAME OF PERFORMING ORGANIZATION N. C. State University	6b. OFFICE SYMBOL (If applicable)
6c. ADDRESS (City, State, and ZIP Code) Department of Mechanical and Areospace Engineering Box 7910, Raleigh, NC 27695-7910	7a. NAME OF MONITORING ORGANIZATION Air Force Office of Scientific Research AFOSR/NA
	7b. ADDRESS (City, State, and ZIP Code) Bolling AFB, D. C. 20332-6448
8a. NAME OF FUNDING / SPONSORING ORGANIZATION Air Force Office of Scientific Research	8b. OFFICE SYMBOL (If applicable) AFOSR/NA
8c. ADDRESS (City, State, and ZIP Code) Bolling AFB, D. C. 20332-6448 NA	9. PROCUREMENT INSTRUMENT IDENTIFICATION NUMBER F49620-92-J-0189
	10. SOURCE OF FUNDING NUMBERS

PROGRAM ELEMENT NO.	PROJECT NO.	TASK NO.	WORK UNIT ACCESSION NO.
6/1621	2307	AS	52

11. TITLE (Include Security Classification)
Time Accurate Computation of Unsteady Inlet Flows with a Dynamic Flow Adaptive Mesh

12. PERSONAL AUTHOR(S)
McRae, D. Scott and Benson, Rusty A.

13a. TYPE OF REPORT	13b. TIME COVERED	14. DATE OF REPORT (Year, Month, Day)	15. PAGE COUNT
Final Technical	FROM 15/03/92 TO 30/06/94	94/Sept. 7	52

16. SUPPLEMENTARY NOTATION

17. COSATI CODES			18. SUBJECT TERMS (Continue on reverse if necessary and identify by block number)
FIELD	GROUP	SUB-GROUP	Computational Fluid Dynamics, Dynamic Adaptive Mesh, Mixed Compression Inlet Unstart, Unsteady Flow

94-31795

19. ABSTRACT (Continue on reverse if necessary and identify by block number)

Research has been performed to obtain very accurate dynamic simulations of supersonic inlet unstart using CFD codes and a dynamic solution adaptive mesh algorithm developed at NCSU. The codes use Runge-Kutta time differencing and Advective Upwind Split Method spatial differencing in finite volume form. Other changes have been incorporated to improve the time accuracy when the computational mesh is dynamically adapted. Solutions have been obtained and animated for unstart of generic 2-D mixed compressions and fully supersonic inlets. Analysis of results revealed that laminar viscous flow unstart occurs by a separation/oblique shock mechanism rather than movement of a normal shock. Turbulent flow simulations reveal that initial shock motion occurs initially but then reverts to the separation/oblique shock mechanisms. 3-D steady and unsteady simulations are presented and conclusions drawn concerning the role of separation in inlet unstart.

20. DISTRIBUTION / AVAILABILITY OF ABSTRACT	21. ABSTRACT SECURITY CLASSIFICATION
☒ UNCLASSIFIED/UNLIMITED ☐ SAME AS RPT. ☐ DTIC USERS	

22a. NAME OF RESPONSIBLE INDIVIDUAL	22b. TELEPHONE (Include Area Code)	22c. OFFICE SYMBOL
DR L. SAKELL	202-767-4935	AFOSR/NA

DD FORM 1473, 84 MAR 83 APR edition may be used until exhausted. All other editions are obsolete.

SECURITY CLASSIFICATION OF THIS PAGE

UNCLASSIFIED

DISCLAIMER NOTICE

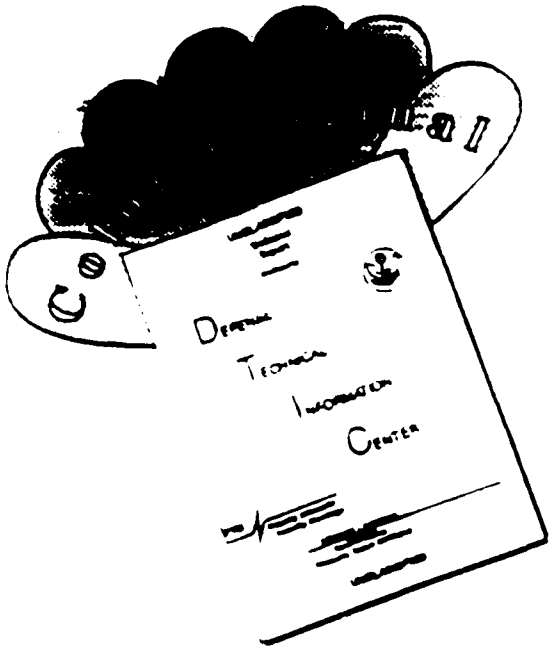

THIS DOCUMENT IS BEST QUALITY AVAILABLE. THE COPY FURNISHED TO DTIC CONTAINED A SIGNIFICANT NUMBER OF COLOR PAGES WHICH DO NOT REPRODUCE LEGIBLY ON BLACK AND WHITE MICROFICHE.

TIME ACCURATE COMPUTATION OF UNSTEADY INLET FLOWS WITH A DYNAMIC FLOW ADAPTIVE MESH

D. Scott McRae
Rusty A. Benson

Department of Mechanical and Aerospace Engineering
North Carolina State University
Raleigh, North Carolina 27695-7910

7 September 1994

Final Report for Period 15 March 1992 - 31 June 1994
AFOSR Grant F49620-92-J-0189

Distribution Unlimited

Prepared for

Air Force Office of Scientific Research
AFOSR/NA
Bolling AFB, D. C. 20332-6448

Abstract

Research has been performed to obtain very accurate dynamic simulations of supersonic inlet unstart using CFD codes and a dynamic solution adaptive mesh algorithm (DSAGA3D) developed at NCSU. During the grant period, the codes have been changed to Runge-Kutta time differencing and Advective Upwind Split Method spatial differencing in a full finite volume formulation. Other changes have been incorporated to improve the time accuracy when the computational mesh is dynamically adapted. Solutions have been obtained and animated for unstart of generic 2-D mixed compression and flow through supersonic inlets. Analysis of results revealed that unstart is primarily a viscous phenomena in laminar flow and is propagated by a separation/oblique shock mechanism rather than movement of a normal shock. Turbulent flow simulations reveal that initial movement of the shock does occur but viscous effects soon dominate. The response of generic inlets to changes in both freestream angle of attack and temperature as well as changes in engine face pressure are simulated.

3-D simulations of steady and unsteady flow in supersonic through flow inlets are also presented, as well as a discussion of the effect of compression surface initiated corner vortices on the stability of a terminating shock wave. Conclusions are drawn as to observed unstart mechanisms and their interaction with shock positioning and stabilization ports.

Statement of Work, as set forth in the original proposal

Research will be conducted leading to time-accurate computational solutions for the supersonic inlet unstart phenomena. The following specific tasks and investigations will be undertaken:

1) 3-D computer codes will be developed with an explicit upwind solver and with a relaxation-type implicit upwind solver applied to the full Navier-Stokes equations.

2) The dynamic flow adaptive mesh algorithm of Benson and McRae will be installed in these codes to allow increased solution accuracy.

3) Research will be conducted into the source of computational errors in the solutions obtained using moving mesh and into means of avoiding, correcting or reducing these errors.

4) Criteria for mesh quality will be developed based on comparison of the computational results with the various types and sizes of mesh cells. These criteria will then be used to develop means of processing the adaptive mesh weight function to ensure that the mesh quality is optimum.

5) A high level graphics work station will be purchased and used to animate the time accurate results for analysis. Research using this device will be conducted into the real time capture and animation of the computed results to allow monitoring and analysis of the computation while in progress.

6) Finally, the capability to compute time and spatially accurate flow fields will be demonstrated by several demonstration cases, to be determined by consultation with AFOSR or a designated AF Laboratory and by the amount of available computer resources.

TASKS ACCOMPLISHED

Code Development

Upon initiation of this grant, 2-D and 3-D codes in finite difference form were operational using MacCormack's algorithm with either standard MacCormacks dissipation or Kwak and Yoon 2nd/4th order dissipation and our dynamic flow adaptive mesh algorithm[1,2,3] with mesh velocity included in the integration for time accuracy. Initial inlet solutions obtained with these codes indicated that the stability and dispersion characteristics were not suitable for the very complex shock and separation systems present during unstart. Because of these early results, the decision was made to investigate upwind methods in order to improve computed results and code stability.

Roe's flux difference splitting scheme was coded initially. However, the interaction of the mesh velocity metric derivatives with Roe's flux difference splitting method proved to cause problems as initially coded. It was apparent that considerable development was going to be required in order to obtain a time accurate flux difference splitting method for the moving mesh. As an alternative, flux-vector splitting techniques incorporate the mesh velocity metrics in a manner similar to the central difference techniques. Unfortunately, these techniques typically produce excess dissipation which causes inaccurate solutions for viscous flows.

We did find, however, that the hybrid Advective Upwind Split Method (AUSM) of Liou and Steffen[4] had the necessary form of the split flux vector for incorporation of the mesh velocity metrics but without most of the excess dissipation and sonic point problems of the standard Van Leer and Steger-Warming flux vector splitting methods. This reduction in dissipation results primarily from computing the pressure flux separately. A change in the cell interface Mach number computation was necessary, since AUSM as originally published would not allow a normal shock to move upstream for $M \geq 2$ and certain mesh distributions in the shock wave transition. A new interface equation was devised:

$$M_{1/2} = \frac{P_{left} M_{left} + P_{Right} M_{Right}}{P_{left} + P_{Right}}$$

This equation proved to allow correct normal shock movement and did not degrade scheme accuracy. However, more recent work by Liou has shown that the equation:

$$M^{\pm} = 1/2\ [m^{+} + m^{-} \pm |m^{+} + m^{-}|]$$

also corrects this problem and gives additional improvements (± indicates right/left).

In order to increase stability bounds and allow for improved time accuracy if required, a multi-stage Runge-Kutta algorithm was substituted for MacCormacks. The two stage version of this algorithm has a theoretical allowable stability limit of CFL=2. This permits approximately twice the time step allowed by the MacCormack's algorithm but the step is still sufficiently small for time accuracy to be preserved. Higher than second order time accuracy is available with this algorithm if required. The remainder of the code development tasks accomplished during the grant period will be summarized here and addressed in detail as appropriate in following sections.

Analysis of results obtained with the original version of the code revealed that both conservation and time accuracy were not being met, although the percentage error at each time step was small. This problem was reported in the grant interim technical report[5]. The code was then converted to finite volume formulation while still using the AUSM technique. Although it has not proven to produce completely monotamic results, the use of AUSM has reduced greatly adverse interaction with the dynamic mesh algorithm.

As part of the recoding to Runge-Kutta and finite volume formulation, the algorithm was divided into three steps, the third of which served to update the solution for mesh velocity terms in the transformed equations.

The algorithm in this form proceeds for each time integration step:

1) Integration of the steady terms in the governing cognation using mesh locations obtained in the previous time step.
2) Based on weight functions obtained from the solution of step 1), the mesh is adapted to the solution.

3) The final result is obtained by integrating the grid velocity terms in the transformed equation using the results of steps 1) and 2).

Step 3) was initially coded as a Taylor series expansion[5]. This did serve to increase time accuracy but satisfactory time accuracy was still not achieved. As noted below, this problem has been improved greatly by substitution of a Runge Kutta integration for step 3) and recoding the grid velocity change as a change in cell volume with respect to time. The result is improved time accuracy, as will be demonstrated below.

Realistic inlet unstart computations require that turbulence be modeled in the code. However, all of the unstarts computed to date have involved massive separations with the unstart mechanism dominated completely by viscous effects. Finding a turbulence model that will give reasonable results for massive unsteady separations has proven to be a difficult task. A standard Baldwin-Lomax[6] model was first coded. This proved to give results that were clearly non-physical in regions of large separation. Goldberg's[7,8] backflow model was then added, with somewhat improved but still inadequate results. Finally, Edwards[9,10] modified Baldwin Barth[11] model was installed. This model gave improved results but has not yet been fully verified and may still need further modification for the 3-D cases.

Boundary conditions were improved throughout the study, with simulated wall bleed added to stabilize the terminating normal shock in mixed compression cases and to reduce separation due to shock-wave boundary-layer interaction at cowl shock wave reflections. The ability to represent dynamic changes in the flow was added at both upstream and downstream boundaries. Solutions were then obtained simulating the effects of both free-stream and engine face conditions.

Time Accuracy

As originally coded, the mesh velocity terms were included in strong conservation law finite difference form and integrated with the remaining components of the flux vectors. Numerical experiments were conducted in which a normal shock of known speed and strength was propagated through a grid, both with and without mesh adaption. The position error of the

computed shock wave as obtained with the original mesh velocity formulation exhibited both a long period oscillation and a position error when the mesh was adapted (Fig. 1). Although the computed shock wave speed was changed by the startup process[5] the speed is clearly continuing to change with time. As noted above, the algorithm was then split into three steps in an attempt to improve time accuracy.

The first step of the three step algorithm was coded in finite volume formulation in order to improve conservation. Step three of the algorithm, as initially coded, begins with a Taylor series expansion in time

$$U^{n+1} = U^{i+1} - \Delta\tau \left(\xi_t^{n+1} U_\xi^{i+1} + \eta_t^{n+1} U_\eta^{i+1} \right)$$

$i+1 \Rightarrow$ last Runge Kutta stage

$n+1 \Rightarrow$ current time level

$$\xi_t^{n+1} = x_\tau^{n+1} \xi_x^{n+1} + y_\tau^{n+1} \xi_y^{n+1}$$

$$\eta_t^{n+1} = x_\tau^{n+1} \eta_x^{n+1} + y_\tau^{n+1} \eta_y^{n+1}$$

$\Delta\tau = \Delta t$ since $\tau = t$ in x-form

$$-\Delta\tau \, \xi_t = \Delta x \, \xi_x + \Delta y \, \xi_y$$

$$-\Delta\tau \, \eta_t = \Delta x \, \eta_x + \Delta y \, \eta_y$$

$$\Delta x^{n+1} = x^{n+1} - x^n$$

$$\Delta y^{n+1} = y^{n+1} - y^n$$

$$U^{n+1} = U^{i+1} + (\Delta x^{n+1} \xi_x^{n+1} + \Delta y^{n+1} \xi_y^{n+1}) U_\xi^{i+1} + (\Delta x^{n+1} \eta_x^{n+1} + \Delta y^{n+1} \eta_y^{n+1}) U_\eta^{i+1}$$

$$U^{n+1} = U^{i+1} + \Delta x^{n+1}(U_\xi^{i+1} \xi_x^{n+1} + U_\eta^{i+1} \eta_x^{n+1}) + \Delta y^{n+1}(U_\xi^{i+1} \xi_y^{n+1} + U_\eta^{i+1} \eta_y^{n+1})$$

which then reduces to:

$$U^{n+1} = U^{i+1} + \Delta x^{n+1} U_x^{i+1} + \Delta y^{n+1} U_y^{i+1}$$

a Taylor series expansion in space. When cast in this form, integration of the mesh velocity terms can be shown to be equivalent to an interpolation of the new dependent variables to the new mesh locations. The interpolation form of this step required fewer operations and therefore was coded. The equivalence of the series expansion in time and the interpolation is a consequence of the fact that the mesh velocity corrects the fluid velocity vector for the relative motion of the computational mesh with respect to the inertial frame.

The above formulation improved solution time accuracy, (Fig. 2), but a long period oscillation in shock position persisted (i.e., the shock speed was not constant when the mesh was adapted).

The next step was to return the algorithm to full conservation finite volume form for the mesh velocity integration as well as to increase the order of accuracy. This approach is similar to that in reference 12 and is best defined by a fundamental examination of conservation laws subject to arbitrarily changing volumes.

A conservation law results from the concept that a quantity or property may be physically conserved in both time and space. The mathematical definition of a conservation law results when the time rate of change of some quantity B summed over a given volume is shown to be equal to a quantity Γ (which may, of course, be zero), or

$$\frac{d}{dt}\int_v B dV = \Gamma$$

In the present application, B is either the density, momentum, or total energy. Applying the theorem of Leibnitz to the equation, two integrals result; one to account for the time rate of change of B summed over the volume and one for the change in B due to motion of the boundary,

$$\frac{d}{dt}\int_v B dV = \int_v \frac{\partial B}{\partial t} dV + \oint_s B\vec{\omega}\cdot d\vec{s} = \Gamma$$

It is common practice to assume the region or volume is not changing with time but only translating in space at the local fluid velocity. With this assumption, $\vec{\omega}$ becomes the local fluid velocity and thus,

$$\frac{d}{dt}\int_v B dV = \int_v \frac{\partial B}{\partial t} dV + \oint_s B(u\,\hat{i} + v\,\hat{j} + w\,\hat{k}) \cdot d\vec{s} = \Gamma$$

The preceeding equation is easily reduced to the familiar form of the conservation laws, which are correct only if the volume of interest is fixed in magnitude to that necessary to contain the original mass. However, if the volume is allowed to expand or contract independent of the motion of the fluid particles, then the volume boundaries no longer move at the local fluid velocity and a new reltionship for $\vec{\omega}$ must be determined.

Consider a one-dimensional flow where the boundary of a region is moving with speed $\dot{x}$ and the fluid is moving at a velocity u. In this case, the relative velocity of the system at the interface is $u - \dot{x}$, which is the velocity that should be used in the surface integral resulting from Leibnitz's Rule. Substituting the corresponding definition of $\vec{\omega}$ for a three-dimensional volume into the conservation law after application of Leibnitz's Rule results in

$$\int_v \frac{\partial B}{\partial t} dV - \oint_s B(\dot{x}\,\hat{i} + \dot{y}\,\hat{j} + \dot{z}\,\hat{k}) \cdot d\vec{s} + \oint_s B(u\,\hat{i} + v\,\hat{j} + w\,\hat{k}) \cdot d\vec{s} = \Gamma$$

which is proposed[13] as the correct statement of conservation for an arbitrary volume allowed to expand or contract in time.

If the definition of Γ is substituted and B is redefined to be the vector of properties that are conserved in fluid flow, $U = \left[\rho, \rho\vec{V}, E_t\right]^T$, a more familiar form of the conservation equations can be written.

$$\int_v \frac{\partial U}{\partial t} dV - \oint_s U\vec{x} \cdot d\vec{s} + \oint_s \vec{A} \cdot d\vec{s} = 0$$

$\vec{A}$ is a vector containing the flux components in the cartesian frame, $E\,\hat{i} + F\,\hat{j} + G\,\hat{k}$ and $\dot{x}$ is the speed at which the surface is expanding or contracting, $\dot{x}\,\hat{i} + \dot{y}\,\hat{j} + \dot{z}\,\hat{k}$. In three dimensions, the second integral in this equation represents the change in the conserved quantity U due to the time rate of change of the cell volume. Implementation of this integral in the code has improved the time accuracy as assessed by movement of a shockwave through a grid (Fig. 3).

Also, the same Runge Kutta Algorithm is currently being used to advance both steady and grid movement steps.

Boundary Conditions

Because the equations are expressed in cell-centered finite-volume form, values are not explicitly known at the domain boundaries but at a volume center displaced from the boundary. Therefore, domain boundary conditions are enforced by placing a "ghost volume", a symmetric reflection of a volume abutting the domain boundary, next to the boundary such that the correct conditions are obtained at domain boundaries.

At the inflow boundary, freestream values are specified since all flows considered are fully supersonic. At the outflow boundary, two cases need to be considered. The first is supersonic outflow, in which the dependent varible values are extrapolated to the ghost volume using a zeroth-order extrapolation. For the case of a subsonic outflow, the pressure is chosen to be specified as a ratio to the freestream inlet pressure. All other values at the outflow are calculated by integrating the one-dimensional characteristic relations, after neglecting the equation associated with the negative eigenvalue. The characteristic relations are advanced in time using the multi-stage Runge-Kutta algorithm with one-sided differences in the direction normal to the boundary.

At solid surfaces, the no-slip condition is enforced by placing an equal and opposite velocity vector in the boundary condition array. When an insulated wall is simulated, a temperature is specified. If the wall is determined to be adiabatic, then $(dT/dn|_w = 0)$ is enforced. The pressure is determined using a momentum correction model at wall:

$$dp/dn = - \rho \tilde{V}_N d\tilde{V}_N / dn \ ,$$

where $\tilde{V}_N$ is the velocity normal to the surface. The pressure for the ghost volume is calculated using the relation $p_0 = 2p_{wall} - p_1$. In the presence of a porous bleed boundary, the tangential velocity component is still assumed to be zero and the normal component is determined using a

specified mass flux, $\rho\bar{V}_N$ = const. This bleed model has been used by many researchers with good comparisons to experiment[14,15].

Turbulence Modeling

A standard Baldwin-Lomax[6] turbulence model was installed in the 2-D code and checked through comparison with standard cases. However, as expected, this model proved to give poor results when used for flow conditions that produce massive separations. In order to correct this problem, Goldberg's backflow turbulence model[7,8] was installed in conjunction with the Baldwin-Lomax model, the combination which had been shown to improve results for other separated flow cases. This combination did improve somewhat the Baldwin Barth Results (Fig. 4). However, this model did not allow physically realistic solutions in the case of massive separations or 3-D corner flows due to the difficulty in determining the correct length scale.

An examination of the literature describing two-equation models revealed that the mesh spacing near a wall necessary to provide adequate model behavior was extremely prohibitive ($\hat{n}^+ \approx 0.2$). An alternative to the algebraic and two-equation models is the one-equation model of Baldwin and Barth[11] with the modifications set forth by Edwards[10], and Edwards and Chandra[9].

In the Baldwin and Barth model, a transport equation for the quantity F, defined as k^2/ε, is derived from partially modelled versions of the turbulent kinetic energy, k, and dissipation, ε, equations. In their original paper, Baldwin and Barth present a technique for solving the transport equation for F such that it is decoupled from the Navier-Stokes equation set. The transport equation for F, including the modifications of Edwards, is:

$$B_1\rho\frac{DF}{Dt} = B_2 f_2(D_1, D_2)\sqrt{\rho FP} + \frac{1}{Re}\left[\frac{1}{\sigma R}(\mu + \mu_t)\nabla^2 F - \frac{1}{\sigma_\varepsilon}\frac{\mu_t F}{\hat{n}^2}\right]$$

The turbulent eddy viscosity is then obtained from the relation:

$$\mu_t = \rho C_\mu F D_1 D_2$$

where D_1 and D_2 are wall damping functions and $f_2(D_1, D_2)$ is a term to reduce production near the wall.

For the current application, F was treated as another field equation and advanced in time using the Runge-Kutta algorithm. To accomplish this, the equation was recast into strong conservation law form and is similar to the momentum equation with an added source term. The resulting non-dimensional equation in cartesian coordinates is:

$$\frac{\partial \rho F}{\partial t} + \frac{\partial}{\partial x}\left(\rho u F - \frac{\mu + \mu_t}{\sigma_R B_1 Re}\frac{\partial F}{\partial x}\right) + \frac{\partial}{\partial y}\left(\rho v F - \frac{\mu + \mu_t}{\sigma_R B_1 Re}\frac{\partial F}{\partial y}\right)$$

$$= \frac{1}{B_1}\left[B_2 f_2(D_1, D_2)\sqrt{\rho F p} - \nabla\frac{\mu + \mu_t}{\sigma_R Re}\cdot\nabla F - \frac{\mu_t F}{Re\sigma_e \hat{n}^2}\right]$$

where

$$P = \frac{\mu_t}{2} S_{ij} S_{ij},$$

$$f_2(D_1, D_2) = \left(\frac{1}{\kappa \hat{n}^+} + D_1 D_2\right)\sqrt{D_1 D_2},$$

$$D_i = 1 - \exp\left(\frac{-\hat{n}^+}{C^+_i}\right),$$

$$\hat{n}^+ = \frac{\rho}{\mu}\left(\frac{C_\mu F}{\kappa} + 0.0055\sqrt{u^2 + v^2 + w^2}\,\hat{n} Re\right),$$

$$\frac{1}{\sigma_\varepsilon} = \frac{B_2\sqrt{C_\mu}}{\kappa^2}, \qquad \frac{1}{\sigma_R} = 1.64\left(\frac{1}{\sigma_\varepsilon}\right)$$

$$B_1 = 0.95, \qquad B_2 = 1.00$$

$$C_1^+ = 19.0, \qquad C_2^+ = 12.0$$

$$C_\mu = 0.09, \qquad \kappa = 0.41$$

Values for B_1, B_2, C_2^+, and C_2^+ are those currently used by Edwards and Chandra[9] and agree well when compared with the compressible law-of-the-wall[16] and Cebeci-Smith[17] outer layer formulation. When two or more walls are considered, the normal distance, $\hat{n}$, and the corresponding

wall coordinate, $\hat{n}^+$, are taken to be the minimums of the computed values to each wall. The equation is transformed into computational coordinates prior to use. The only boundary conditions required for the Baldwin and Barth turbulence model are a prescribed freestream value, $F = 0.1$, and that the turbulence vanish at wall surfaces (either porous or solid).

Adaptive Mesh Algorithm

Improvements have been made in the implementation and coding of the adaptive mesh algorithm. Also, the first steps toward extending the adaptive mesh algorithm to multiple blocks were completed during the first year of the grant period and was illustrated in the interim report[5]. In this case, a second grid block was placed above the cowl. Adaption in this case was possible only in the η direction because of difficulty with adapting the mesh in the ξ direction while maintaining continuous mesh lines as they translate out of the inlet and off of the cowl lip. Our initial analysis indicates that block boundaries must allow, in some instances, discontinuous mesh lines in order to correct this problem in general configurations. Inlets with bleed ports will also require a discontinuous mesh at block boundaries if full adaption is to be used in each block, since adjacent blocks will have widely varying numbers of mesh lines. We have developed, under separate funding, techniques to adapt the block boundaries along with interior points for certain configurations of adjacent blocks with continuous mesh lines, but have not incorporated this technique in the inlet codes. We expected to include adapted block boundaries during the grant period, but the multiblock research did not achieve sufficient maturity or time accuracy to warrant incorporation.

Experimental Verification

The acquisition of experimental inlet unstart data for verification of our computations has proven much more difficult than we expected because of our university requirement that student research must be published in the open literature. To date, we have not obtained suitable data that could be openly published. Current dynamic inlet data seem to fall into two categories:

1) Those which are restricted due to being NASP-related. 2) Those which are deemed sensitive due to international competitiveness concerns. Virtually all of the supersonic through flow data being taken currently by NASA falls into one of these categories.

In our search for dynamic inlet data, we have contacted Pratt and Whitney Aircraft (West Palm Beach), The Air Force Propulsion Laboratory, and the NASA Ames, Langley and Lewis Research Centers. The majority of the dynamic inlet data is being taken at NASA Lewis, with some before and after (but not during) unstart data taken at NASA Langley.

NASA Lewis offered access to their unclassified data if we agreed to shield the data from foreign nationals and to delay publication for 2 to 3 years. We petitioned the Dean of the Graduate School to set up procedures to allow our participation in these and other restricted NASA research endeavors. However, this petition was deemed to be in opposition to the concept of academic freedom and was denied.

We are grateful to the Experimental Hypersonics Branch at NASA Langley for agreeing to conduct cooperatively generic dynamic inlet unstart experiments in their M=6, 15 inch and 20 inch wind tunnels. We are working with Dr. Scott Holland of the branch on these experiments. We have designed, at NCSU, an essentially 2-D generic inlet which is being constructed with glass side walls to allow high speed Schlieren photography and with dynamic pressure and temperature transducers on the opaque surfaces. The final design is similar to the generic 2-D inlets for which we have obtained dynamic and static solutions. The major changes were a radius at the throat for ease in machining and a movable exit plug with exit contouring to allow controlled unstart of the inlet. Starting of the inlet is assisted by a movable cowl surface to increase throat area.

A blockage model was constructed to ensure that the tunnel would not be choked and to confirm the design. The data reort from the blockage tests will be available soon. Examination of standard frame rate Schlieren video taken during these tests reveals that the design will start under all but the lowest laminar Reynolds numbers and that the plug, after some shimming, is effective in unstarting the inlet. The windows on this initial model were not full size, but the unstarted shock patterns that were visible matched qualitatively those seen in our computations.

We anticipate that construction of the final model and tunnel entry will occur in the last quarter of FY95.

Results

As noted in the interim grant report, presentation of dynamic results in report form is difficult. This difficulty is compounded in the final report by the need to illustrate the heretofore unnoted inlet unstart mechanisms that were identified in the course of the research. We will present sufficient sequenced stills to demonstrate the increased dynamic resolution achieved through the dynamic adaptive grid algorithm and to illustrate the manner in which the unstarts are initiated and propagate through the inlet. Cases will also be presented which show response of generic inlets to rapid free stream changes, such as would result from aircraft attitude transients and static temperature variations. The observed unstart mechanisms will be reviewed first in order that each can be discussed as it is presented.

The classical mechanism of mixed compression inlet unstart, as usually noted in basic texts, consists of the terminating normal shock wave being destabilized by some change in conditions and traversing through the throat of the inlet to the entrance. The shock wave then remains at the entrance (resulting in low total pressure recovery at the engine face) or is repeatedly reingested and disgorged in the phenomena known as inlet "buzz". We have been able to obtain a clearly identifiable classic unstart mechanism only for inviscid flow. Instead, for all of the cases where viscous effects were present, flow separation has been the mechanism of propagation of the unstart. For turbulent flow conditions, the reduced tendency to separation permits some terminal shock movement; however, the viscous separation soon outpaces the shock movement.

The mechanism that is common to all laminar cases for our generic inlets is separation at the base of the terminal shock after the shock moves away from the stabilizing bleed region. An oblique shock forms at the leading edge of the separation and this shock/separation system proceeds rapidly upstream at a velocity greater than the shock velocity. This same mechanism occurs on the compression surface side for turbulent flow conditions, but the shock/separation

system moves forward at smaller velocity compared to the shock speed. The cowl side of the inlet, which in our designs has a smaller adverse pressure gradient, does not consistently separate under turbulent flow conditions.

Results obtained for our most recent 2-D design (for turbulent conditions) also illustrated that separation can occur upstream of the normal shock at very weak wave reflections. Detailed examination of animated velocity vectors reveals that unstart occurs very rapidly after the flow separates. These mechanisms will be noted as we discuss each case in turn.

2-D Generic Inlet Unstart

Early unstart results obtained for a generic 2-D inlet under both inviscid and viscous conditions were presented at the AIAA 10th Applied Aerodynamics meeting[18]. Figure 5 shows M=3, second order accurate inviscid results for the latter stages of an inlet unstart that was initiated by increasing the back pressure with the exit plane in supersonic flow. Density contours are presented to the right and the corresponding dynamically clustered grids are presented on the left. The expected normal shock originated at the downstream boundary and is moving upstream, with the mesh dynamically resolving it. This case is relatively uneventful until the normal shock encounters the throat and the shock reflected from the inlet cowl lip. The change in sign of vorticity and the strength of the slip surface causes an inviscid vortex to form which is convected downstream. The computation is terminated when the normal shock reaches the cowl lip. This is an excellent example of the classic unstart mechanism until the traveling shock waves reaches the throat and the inviscid vortex is produced.

This configuration[18] was then converged with first order accuracy for laminar viscous supersonic flow at M=3 and $Re=2\times10^5$ with adiabatic wall conditions. We encountered our first problem with outflow boundary conditions when we attempted to unstart this viscous case by increasing back pressure at the exit as we had done with the inviscid flow. The boundary layer separated at the wall, resulting in back flow from the exit plane into the interior[5]. These separations tended to cause numerical instability at the outflow plane or become large such that displacement prevented the flow from becoming subsonic at the exit plane. We have not yet

found a technique for implementing well posed exit boundary conditions in order to maintain stability for all cases of combined subsonic inflow and outflow. Instead, in later runs, standard subsonic boundary conditions were imposed and the back pressure was increased at a slower rate.

We then instantaneously imposed a normal shock upstream of the exit plane with uniform flow conditions between the shock and the exit. Conditions across the shock were set to P_b/P_∞=30. This would correspond to conditions existing after strong bleed is removed at and downstream of the normal shock. The series of plots[18] in Figures 6a and 6b shows that separations with attendant oblique shocks immediately form at the shock-wall intersections. These oblique shock-separation systems then move rapidly upstream, with the separation bubble becoming very elongated as this occurs. Note that the position of the normal shock remains relatively constant, with the strength gradually reduced by the effects of the oblique shock system now propagating upstream. Another interesting point is that the lower oblique propagating shock does not move past the throat. Instead, the separation associated with this shock coalesces with the separation due to the cowl shock resulting in a sudden increase in extent of the cowl shock separation (τ=9.42 and 10.34 in the figure). A strong oblique shock then forms at this enlarged separation and the system then propagates forward. While this is occurring, breakup of the massive separations downstream of the throat results in a series of converging-diverging nozzles with alternating supersonic and subsonic flow. Figures 7a and 7b, which correspond with the Mach contours shown in 6a and 6b, show the adaption of the mesh as it evolves during this unstart.

All of the laminar viscous unstart cases that we have simulated to date have exhibited this oblique shock-separation behavior. The classic model of a normal shock moving forward apparently exists under laminar conditions only in case of "hammer shock" (when flow is essentially stopped at the exit plane) or in the presence of strong bleed. We have found few references to the oblique shock unstart mechanism in the literature, other than brief mention in an early paper by Wieting[19]. We therefore believe that the actual unstart mechanisms of mixed

compression inlets may not be widely understood and that our video animations of the unstarts may promote better understanding of these phenomena.

Results for turbulent flow were first obtained using a Baldwin-Lomax[6] model with Goldbergs[11] back flow model added to improve results for massively separated regions. This combination gave reasonable results in 2-D but was unusable in 3-D due to difficulties in corners. The case shown in Figure 8 was presented[19] at the 29th Joint Propulsion Conference in June 1993. Conditions were M=3, $Re_\infty=3\times10^6$, and abiabatic wall conditions with $T_\infty=100°K$. Unstart was initiated by a back pressure change from $13.75P_\infty$ to $18P_\infty$ over 0.1 ms. As can be seen in the figure, the separation initiated on the diverging surface of the inlet and moved forward rapidly. As the separation increased in size, the combination of the traveling oblique shock and displacement effects caused the disappearance of the original normal shock and the reappearance of a new normal shock at the end of a supersonic "tongue".

After installation of the Baldwin Barth[11] turbulence model as modified by Edwards[10], the code was modified to allow free stream transients in order to assess the effect of these changes on inlet stability. Also, an M=3 inlet was designed for a throat Mach number of ~1.3 with a more realistically contoured throat region. Results were obtained for a 1° angle of attack change, a 2.3°K freestream temperature change, and a back pressure change of 10%. It should be noted that 0.5° angle of attack change and 1.15°K freestream temperature change did not cause unstart. Bleed regions were used at the terminating normal shock and at the intersection of the cowl shock with approximately 3.6% of the inlet entrance flow removed.

The series presented[20] in Figure 9 shows the response of the redesigned generic M=3 inlet geometry to a freestream onset angle change of –1.0 degree. The first image in the series (5 ms, note that $t_c=1$ in the figure) depicts the flowfield just as the inlet reaches the final angle of attack of one degree. This change caused the cowl shockwave reflection and its oblique shockwave train to increase in strength, resulting in a decrease in the Mach number at the throat (7.22 ms). As the simulation progresses, the cowl shockwave angle increases until it intersects the precompression surface ahead of the cowl shock bleed location and a separation bubble forms (8.71 ms). A weak terminating shockwave forms at the end of the oblique shockwave train (9,70

ms) and the throat Mach number falls below unity. The cowl shockwave induced separation expands in extent axially and an oblique shockwave forms at the front of the separation as it translates forward (10.19 ms). The terminating normal shockwave, which has been slowly translating towards the throat, begins to decrease in strength as it reaches the throat (10.70 ms). As the separation bubble increases in size, the oblique shockwave translates forward and interacts with the cowl shockwave to form first a crossing shockwave structure (11.09 ms) and then a single lambda shockwave (11.48 ms) which is about to be expelled from the inlet. During this time, another terminating normal shockwave has formed ahead of the throat and is also translating forward to the inlet entrance. The shock pattern existing at the final stage of the computation is similar to that observed at NASA Langley in the blockage model when unstarted.

Comparing the grids that correspond to each of the contour plots, it can be seen that the adaption algorithm is responding to the movement of the unsteady features as well as continuing to resolve the steady features. All primary characteristics of the flow are detected and mesh points are redistributed to improve the spatial resolution of the unsteady features.

Figures 10 through 15 depict the response of the inlet geometry of the previous case to a temperature perturbation of 2.3K or 2.3% of freestream[20]. The first image in the series (Figure 10) depicts the flowfield in the inlet 0.33 ms after the freestream temperature has reached its maximum value. Figure 11 shows a detail of the throat region with velocity vectors included at every other mesh point in both directions for flow visualization. Note that the color map is reversed in the detail views so that the viscous layer is more visible. Also, the y coordinate is expanded by ~1.6. As the Mach number at the throat is reduced by the change in angle of the cowl shockwave and its oblique shockwave train of reflections, the terminating normal shockwave translates relatively slowly forward through the throat. As the terminating normal shockwave translates forward, the boundary layer thickens as the Mach number upstream of the throat is reduced. Although a weak lambda system forms at the base of the shock as it translates forward, no separation occurs until the shock is at a location approximately midway between the throat and the cowl shock reflection. Separation then occurs and a typical oblique shock/separation system forms and propagates upstream very rapidly. Figures 12 and 13 depict

the overall flow field and the throat detail at a time (16.46 ms) just after separation has occured. Approximately 10.5 ms elapsed prior to separation; the remainder of the unstart required only ~3 ms. Figures 14 and 15 depict the flow field and throat detail when the lambda shock system reaches the cowl lip. During this time, another terminating normal shockwave has formed ahead of the throat and is also translating forward to the inlet entrance.

This case provides an excellent illustration of the effect of separation on inlet unstart. We must surmise that return to stable flow would have been much easier to effect prior to separation. We also suspect that devices such as the vortex valve bleed as used by Paynter[21] would be ineffectual if separation occurs on the compression surface (opposite the bleed port) side of the inlet.

As was seen in the onset angle change, the grid for each of the contour plots shows the adaption algorithm responding to the movement of the unsteady features while still resolving the steady features.

It should be noted that although the two unstarts are different in that the first is driven by cowl shockwave instabilities and the second is similar to a classical unstart, the flowfields are almost identical once the initial compression surface boundary layer separates. The final image for each case contains a lambda shockwave, a massive separation of the initial compression surface boundary layer, a terminating normal shockwave between the lambda shockwave structure and the throat of the inlet, and thick boundary layers in the diffuser portion of the geometry. Note that in both instances, the shockwaves are continuing to move forward at the final instant presented. The computations were terminated at the time that the lambda shockwave structure reached the cowl-lip, since no external mesh was present to allow inlet flow spillage.

3-D Inlet Cases

We have found it difficult to stabilize a terminating shock in our generic 3-D designs. The difficulty occurs primarily due to the corner vortices which must arise at the intersection of the first compression surface and the sidewall and due to weak crossing shocks which are caused

by sidewall boundary layers. These 3-D features effectively result in larger volumes of low momentum/mach flow in the throat region than would exist with a normal attached boundary layer. For the 2-D inlets, usual practice involved inserting numerically, into a converged supersonic flow through solution, a terminating normal shock wave at the aft bleed location and then reconverging the solution. Since the flow downstream of the throat is not uniform, the shock is no longer planar normal to the inlet centerline after reconvergence. (Note that we cannot initiate a shock at the downstream exit and move it forward as the inlet would spontaneously unstart due to separations at the shock wave boundary layer interaction). When the shock insertion procedure was applied to the generic 3-D inlets, the inserted terminating shock would become very skewed and the inlet would spontaneously unstart. Since each attempt to stabilize the terminating shock wave required large amounts of CPU and calendar time (wait time in large-memory queues) and since the unstarts would not have been useful unless time accurate, we chose to place emphasis first on achieving time accuracy and second on demonstrating the efficacy of the code for supersonic and hypersonic through flow type inlets.

The vortices and downstream corner structure noted above can be observed very clearly in our steady numerical solution for a M=10 generic hypersonic inlet tested experimentally at NASA Langley by Holland[22]. The geometry of this inlet can be inferred from Figure 16 which depicts the original unadapted mesh on the solid surfaces with symmetry plane nearest to the observer. Figure 17 depicts both mesh and mach contours[13], with the geometry expanded by a factor of ~2.6 in the smallest throat dimension for clarity. Note that the vortices originating in the compression corners are still intact at the exit plane and are quite strong. Note also the large vortices near the centerline due to the crossing shock interaction. We now understand why large bleed flow percentages are often quoted for rectangular cross section inlets. The adaptive mesh algorithm assists analysis of this flow by resolving these features so their true extent and strength is apparent. Figure 18 shows an expanded view of the exit plane, again illustrating these vortices.

The final case considered is the fully-turbulent flow through a three-dimensional mixed-compression inlet. The inlet geometry was one of many simulated by Korte, et al.[23] as part of a

performance enhancement study with the goal of designing a wind tunnel model. The geometry and an analysis of the steady-state flowfield are presented in reference [23]. The freestream conditions given are a Mach number of 4, a Reynolds number based on the length of the inlet of $48.17(10^6)$, and a freestream temperature of 70°K. In the present study[24], the response of the steady flowfield in the inlet to an instantaneous change in yaw angle is simulated. The results presented are included as a demonstration of the dynamic solution-adaption grid algorithm in three dimensions as well as the modified Runge-Kutta algorithm. The computation was not continued to ascertain whether inlet unstart would occur.

The initial grid for this case has 90 nodes in the streamwise direction (35 of which are in the throat section), 41 nodes in the normal direction and 62 nodes in the transverse direction. Shown in figure 19 are the adaptive grid and pressure contours that exist in the inlet just prior to the yaw angle being introduced at the freestream plane. In these plots, the transverse coordinate has been stretched by a factor of two to aid in visualization. Note that the mesh has redistributed nodes for capturing the crossing oblique shockwave train.

Figure 20 depicts a series of grid and pressure contour plots at three different times after the yaw angle of 5.5 degrees has been introduced at the freestream plane of the grid. The cowl plane, which corresponds to the bottom plane of the finite-volume grid, is chosen for visualization of the effect of this yaw angle change. The first image in each of the series shows adapted grid and pressure contours for the unperturbed freestream. The second and third images in each of the series show the grid and pressure contours after the disturbance translates approximately one-third and two-thirds of the way through the domain, respectively. Although insufficient grid cells are present in the streamwise direction for adequate shockwave resolution in the region upstream of the throat, the grid algorithm is tracking the disturbance and redistributing cells as the shockwave structure is altered by the new freestream. The apparent alteration of the boundary surfaces in the figure is caused by the fact that the centers of the finite-volume grid are being plotted and not the cell-vertices. DSAGA3D does not alter the definition of the boundary surfaces.

VISUALIZATION AND ANIMATION

As provided by the terms of the grant, we purchased a Silicon Graphics Inc. Iris 440/VGX Power Series workstation. Price reductions in CPU, memory and disk between the original quotes and final approval of the grant allowed purchase of 256 MBytes of memory and 25 GBytes of disk space for this system. This additional storage has proven to be very beneficial to animation of the unsteady flow results. We also purchased a V-LAN Receiver and video recording equipment to allow frame accurate recording of video images in VHS and S-VHS format. An FDDI Communications board is also installed but has only been in operation for portions of the grant period due to continuing changes in the campus network.

Our original goal was to automate completely the graphic rendering and animation process, so that it would take place in background on our 440 VGX. If successful, this would allow spot checking of the visualization and code development to take place while the animation images are being created and recorded on video tape. We have been successful in some automation of the process, but have not yet achieved the stated goal. We originally used NASA's Flow Analysis Software Tool kit (FAST) to generate the graphical images but found that it would not execute in background, resulting in excessive rendering time per image (1 to 2 minutes). The developers of FAST at NASA Ames were unable to provide a solution to this difficulty.

We have found that the graphical analysis package TECPLOT (Ametek Eng. Inc.) is much faster (than FAST), produces higher quality images, will run in background allowing work station usage for other purposes and has reduced our elapsed time to render images by at least a factor of five.

Animation of the unsteady solutions has proven to be essential for analysis and understanding of the unsteady results. As an example, the PI examined the computational results of the 2-D free stream temperature transient case using Tecplot and the plot style of figures 11, 13 and 15 to plot selected time steps prior to full animation. The stride chosen, however, completely skipped the prethroat separation and subsequent rapid forward propagation of the

unstart. Instead, for all frames examined, the flow appeared to be attached between the cowl shock reflection and the inlet throat. If no further analysis had been conducted, this case would therefore have appeared to be an exception to our finding that the unstarts are viscously dominated. However, once the case was fully animated with velocity vectors included, it was apparent that separation occurred and that the "plot selected intervals" approach simply missed the most important feature of the results.

Video animation also makes key findings and important issues easily accessible to those who have not beem intimately involved with the research. All who have viewed the unstart animations have agreed with our conclusion that viscous effects dominate the unstart mechanism for our generic inlets.

COMPUTER RESOURCES

The North Carolina Supercomputer Center (NCSC) has granted 1025 CRAY Y-MP cpu hours for the conduct of this research. In addition, computer resources have been supplied by the USAE Waterways Experiment Station computer facility under sponsorship of AFOSR. The investigators are grateful for this support of our work, which would not have been possible otherwise.

COOPERATIVE EFFORTS

A cooperative program, mixed compression inlet stability research, has been discussed with Boeing Aircraft Co. NASA Lewis would also be a participant in this program. No final agreement on this program has been obtained. (Letter, Boeing Commercial Airplane Co., attached).

PARTICIPATING PROFESSIONAL PERSONNEL

D. Scott McRae, Professor
Rusty A. Benson, Research Assistant
Michael Neaves, Research Assistant
Department of Mechanical and Aerospace Engineering
N. C. State University
Raleigh, North Carolina 27695-7910

PUBLICATIONS

Benson, R. A., McRae, D. S., and Edwards, J. R., "Numerical Simulations Using a Dynamic Solution-Adaptive Grid Algorithm, with Applications to Unsteady Internal Flows", AIAA Paper 92-2719, 10th Applied Aerodynamics Conference, Palo Alto, CA, June 1992.

Benson, R. A. and McRae, D. S., "Numerical Simulations of the Unstart Phenomena in a Supersonic Inlet/Diffuser, AIAA 93-2239, AIAA 29th Joint Propulsion Conference, Monterey, CA, June 1993.

Benson, R. A. and McRae, D. S., "Unsteady Transients in a Supersonic Inlet Subject to Freestream Perturbations and Dynamic Attitude Changes", AIAA 94-0581, 32nd Aerospace Sciences Meeting, Reno, NV, Jan. 1994.

Benson, R. A. and McRae, D. S., "Time Accurate Simulation of Unsteady Flows with a Dynamic Solution Adaptive Mesh", Proceedings of the 4th International Conference on Numerical Grid Generation in Computational Fluid Dynamics and Related Fields, Swansea, U.K., April 1994.

McRae, D. S., "Time Accurate Computation of Inlet Unstart," Proceedings of the AFOSR Workshop on Fluid Dynamics of High Speed Inlets, Rutgers Univ., New Brunswick, N. J., 24-25 May 1994.

Benson, R. A., "Development of a Time Accurate Solution Algorithm Coupled with a Dynamic Solution on Adaptive Grid Algorithm with Application to Generic Inlet/Diffuser Configurations," Doctoral Dissertation, Department of Mechanical and Aerospace Engineering, N. C. State University, Raleigh, NC, Jan 1994.

INTERACTIONS

Seminar on the inlet unstart research by McRae and Benson at NASA Lewis Research Center, August 1992.

Discussion of cooperative inlet unstart experiment with The Experimental Hypersonic Branch, NASA Langley Research Center, Dr. Scott Holland.

Discussions on our results and on the fluid dynamics of inlet unstart with Dr. Gerald Paynter, Boeing Commercial Aircraft Co.

The video animations of inlet unstart produced during this research have been incorporated into MAE 465, Propulsion II, our second undergraduate course in Aircraft Propulsion.

SUMMARY AND CONCLUSIONS

A computer code has been developed for the time accurate compution of unstart and other unsteady phenomena in high speed inlets. This code uses DSAGA3D, the NCSU dynamic solution adaptive grid algorithm to automatically enhance resolution of the unsteady processes as the solution evolves. During the grant period, a Runge-Kutta algorithm and AUSM upwinding were installed in finite volume form, and the cell volume time variation term was coded more accurately to improve time accuracy. At the same time, the computational algorithm was divided into three steps in order to couple mesh movement more closely to the solution. After some experimentation with turbulence models, a modified Baldwin-Barth one-equation model was found to give realistic results for separated flows without the computational expense of a two equation model. Time accuracy of the modified code was confirmed through comparison with analytical shock wave motion.

Results were obtained during the grant for unstarts in generic 2-D inlets under inviscid, laminar and turbulent flow conditions. The combination of increased resolution of the unsteady phenomena through the use of dynamic solution adaptive grids and the video animation of the results provided details of the unstart mechanisms not heretofore noted in the literature. The classical notion of unstart by movement of the normal shock was found to be the exception in our results. Instead, the unstart is propagated (and in some instances initiated) by the separation of the viscous layer and the rapid propagation upstream of the resulting oblique shock wave/separation system. This system outpaced the terminating normal shock system in our 2-D generic simulations, although inclusion of turbulent flow simulation retards both separation and the upstream movement of the system once separation occurs. Flow separation was also

ultimately dominant in the unstarts initiated by transients in inlet attitude and free stream temperature. We conclude, therefore, that the prevention of flow separation must be the primary consideration in the design of high speed inlets. It is clear that shock control devices such as the vortex bleed valve would be ineffective in preventing unstart due to separation on the opposite inlet surface as the separation system that causes unstart propagates upstream in the subsonic portion of the viscous layer. Therefore, terminating normal shock movement is not required for the unstart to occur.

3-D simulations revealed a further complication affecting inlet stability. Attempts to stabilize a terminating normal shock in a generic rectangular cross section inlet were unsuccessful at usual bleed rates of 3 to 6% of captured mass flow. The difficulty was primarily caused by the corner vortices which initiate in the intersections of the compression surface and sidewalls. These vortices drastically affected shock contour and position after insertion, causing spontaneous unstart. We conclude that rectangular cross section inlets will require greater bleed percentages in order to reduce the effect of the corner vortices. These corner vortices were well illustrated in the M=10 supersonic 3-D flow through case of Holland. This case also demonstrated the code's usefulness for 3-D steady flows.

The code was also exercised to demonstrate the response of a generic 3-D supersonic through flow inlet to a transient change in attitude. Response and resolution of the dynamic changes were as expected for the mesh size used in the simulation.

We conclude that we have developed a very useful procedure for the analysis of high speed inlet stability and have identified the primary mechanism contributing to inlet unstart. We intend to continue to improve the fidelity of our simulations.

DATA FOR CODE VERIFICATION

The authors respectfully request that DOD and NASA cooperate to select generic configurations in sensitive application areas (such as high speed inlets) and provide published geometry and wind tunnel test data (in particular, unsteady data) that universities can use for student research which must be publishable. The capability to simulate these sensitive

applications will be developed in any case and published, as we have done. The only effect of the competitiveness data restriction is to delay verification of the new simulation techniques and thereby delay the attainment of sufficient confidence in the technique so that they can be used to improve the restricted designs.

REFERENCES

1. Benson, R. A., "A Dynamic Solution-Adaptive Grid Algorithm in Two and Three Dimensions", Masters' Thesis, North Carolina State University, Raleigh, NC, 1989.

2. Benson, R. A. and McRae, D. S., "A Three-Dimensional Dynamic Solution-Adaptive Mesh Algorithm", AIAA Paper 90-1566, June 1990.

3. Benson, R. A. and McRae, D. S., "A Solution-Adaptive Mesh Algorithm for Dynamic/Static Refinement of Two and Three Dimensional Grids", *Proceedings of the Third International Conference on Numerical Grid Generation in Computational Fluid Dynamics and Related Fields*, June 1991.

4. Liou, M.-S. and Steffen Jr., C. J., "A New Flux Splitting Scheme", NASA TM-104404, May 1991.

5. McRae, D. S. and Benson, R. A., "Time Accurate Computation of Unsteady Inlet Flows with a Dynamic Flow Adaptive Mesh," Interim Technical Report, AFOSR Grant F49620-92-J-0189.

6. Baldwin, B. S. and Lomax, H., "Thin Layer Approximation and Algebraic Model for Separated Turbulent Flows", AIAA Paper 78-257, January 1978.

7. Goldberg, U. C., "Separated Flow Treatment with a New Turbulence Model", *AIAA Journal*, Vol. 24, No. 10, Oct. 1986, pp. 1711-1713.

8. Ramakrishnam, S. and Goldberg, U. C., "Versatility of an Algebraic Backflow Turbulence Model", AIAA Paper 90-1485, June 1990.

9. Edwards, J. R. and Chandra, S., "Eddy Viscosity-Transport Turbulence Models for High-Speed Shock Separated Flowfields: Two-Dimensional Results," AIAA Paper 94-0310, Jan. 1994.

10. Edwards, J. R., *Private Communication.*

11. Baldwin, B. S. and Barth, T. J., "A One-Equation Turbulence Transport Model for High Reynolds Number Wall-Bounded Flows," AIAA Paper 91-0610, Jan. 1991.

12. Tamura, Y. and Fujii, K., "Conservation Law for Moving and Transformed Grids," AIAA Conference Paper 93-3365-CP, Orlando, Florida, July 1993.

13. Benson, R. A., "Development of a Time Accurate Solution Algorithm Coupled with a Dynamic Solution on Adaptive Grid Algorithm with Application to Generic Inlet Diffuser Configurations," Doctoral Dissertation, Department of Mechanical and Aerospace Engineering, N. C. State University, Raleigh, NC, Jan. 1994.

14. Talcott Jr., N. A. and Kumar, A., "Two-Dimensional Viscous Simulation of Inlet/Diffuser Flows with Terminal Shocks," *Journal of Propulsion and Power*, Vol. 1, No. 2, March-April 1985, pp. 103-108, 1985.

15. Chyu, W. J., Howe, G. W., and Shih, T. I-P,, "Bleed Boundary Conditions for Numerically Simulated Mixed-Compression Supersonic Inlet Flows," *Journal of Propulsion and Power*, Vol. 8, No. 4, pp. 862-868, July-Aug. 1992.

16. van Driest, E. R., "Turbulent Boundary Layer in Compressible Fluids," *Journal of the Aeronautical Sciences*, Vol. 18, No. 5, pp. 145-160, 1951.

17. Cebeci, T., Smith, A. M. O., and Mosinskis, G. "Calculation of Compressible Adiabatic Turbulent Boundary Layers," AIAA Paper 69-687.

18. Benson, R. A., McRae, D. S., and Edwards, J. R., "Numerical Simulations Using a Dynamic Solution-Adaptive Grid Algorithm, with Applications to Unsteady Internal Flows", AIAA Preprint 92-2719, AIAA 10th Applied Aerodynamics Meeting, Monterey, CA, June 1992.

19. Wieting, Allan R., "Exploratory Study of Transient Unstart Phenomena In a Three-Dimensional Fixed-Geometry Scramjet Engine", NASA TN D-8156, April 1976.

20. Benson, R. A. and McRae, D. S., "Unsteady Transients in a Supersonic Inlet Subject to Freestream Perturbations and Dynamic Attitude Changes", AIAA 94-0581, 32nd Aerospace Sciences Meeting, Reno, NV, Jan. 1994.

21. Paynter, G., "Progress Toward Unsteady Inlet Flow Analysis," Proceedings of the AFOSR Workshop on Fluid Dynamics of High Speed Inlets, Rutgers Univ., New Brunswick, NJ, 24-25 May 1994.

22. Holland, S. D., "A Computational and Experimental Investigation of a Three-Dimensional Hypersonic Scramjet Inlet Flow Field," Ph.D. Disseration, North Carolina State University, June 1991.

23. Korte, J. J., Singh, D. J., Kumar, A., and Auslender, A. H., "Numerical Study of the Performance of Swept, Curved Compression Surface Scramjet Inlets," AIAA Paper 93-1837, June 1993.

24. Benson, R. A. and McRae, D. S., "Time Accurate Simulation of Unsteady Flows with a Dynamic Solution Adaptive Mesh", Proceedings of the 4th International Conference on Numerical Grid Generation in Computational Fluid Dynamics and Related Fields, Swansea, U.K., April 1994.

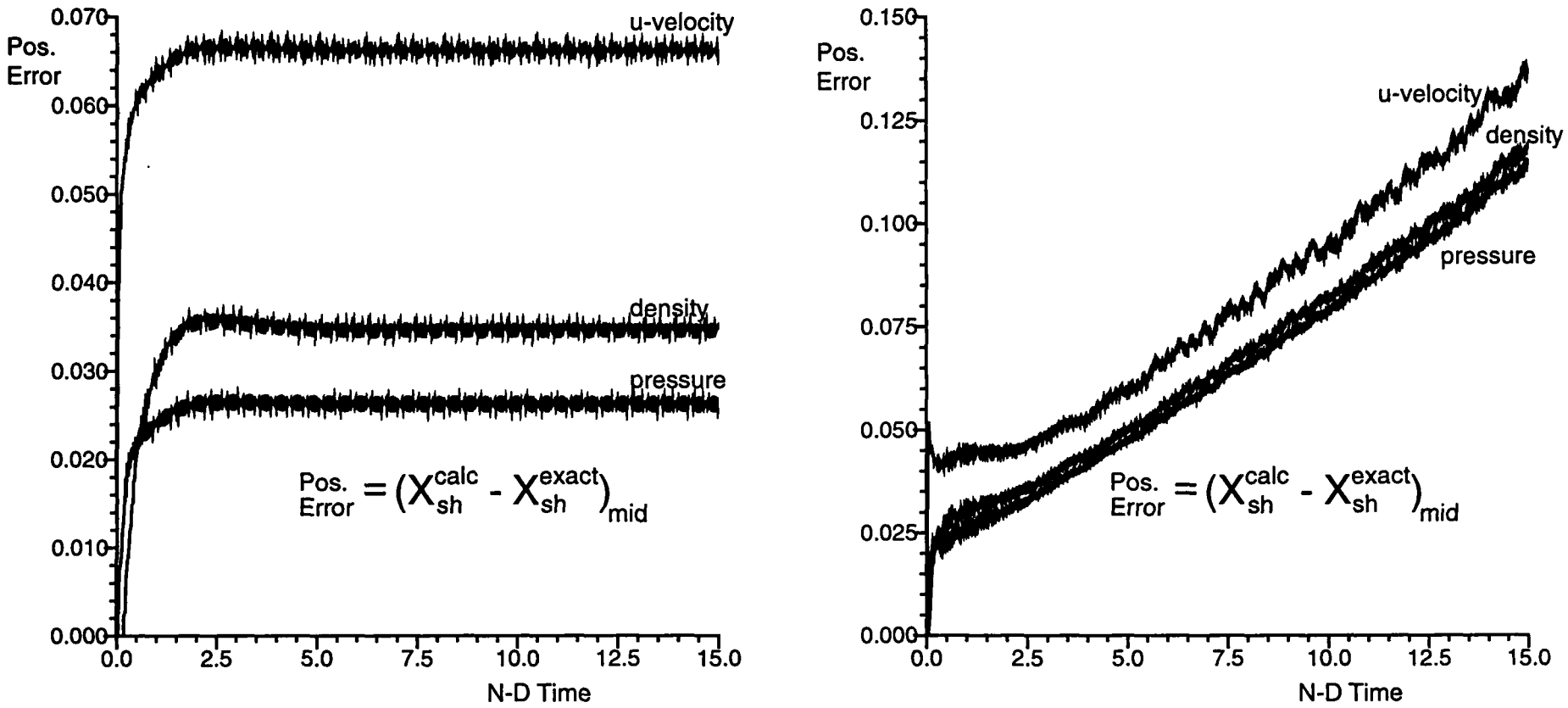

Figure 1: Shock position error for the u-velocity, density, and pressure shocks for the a) unadapted and b) adapted (M_s=10)

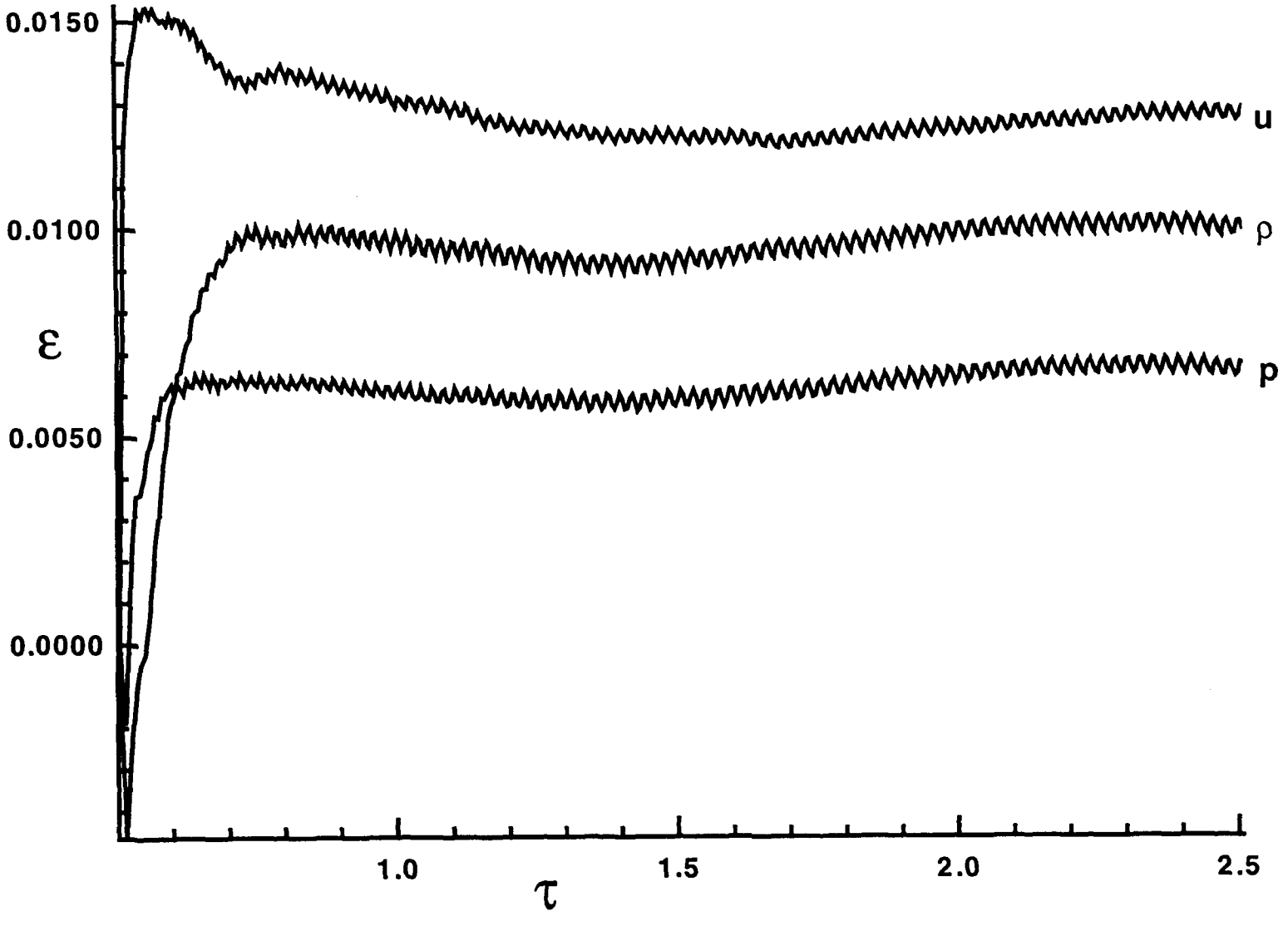

Figure 2: Shock position errors versus non-dimensional time for the adapted grid (M_s=10)

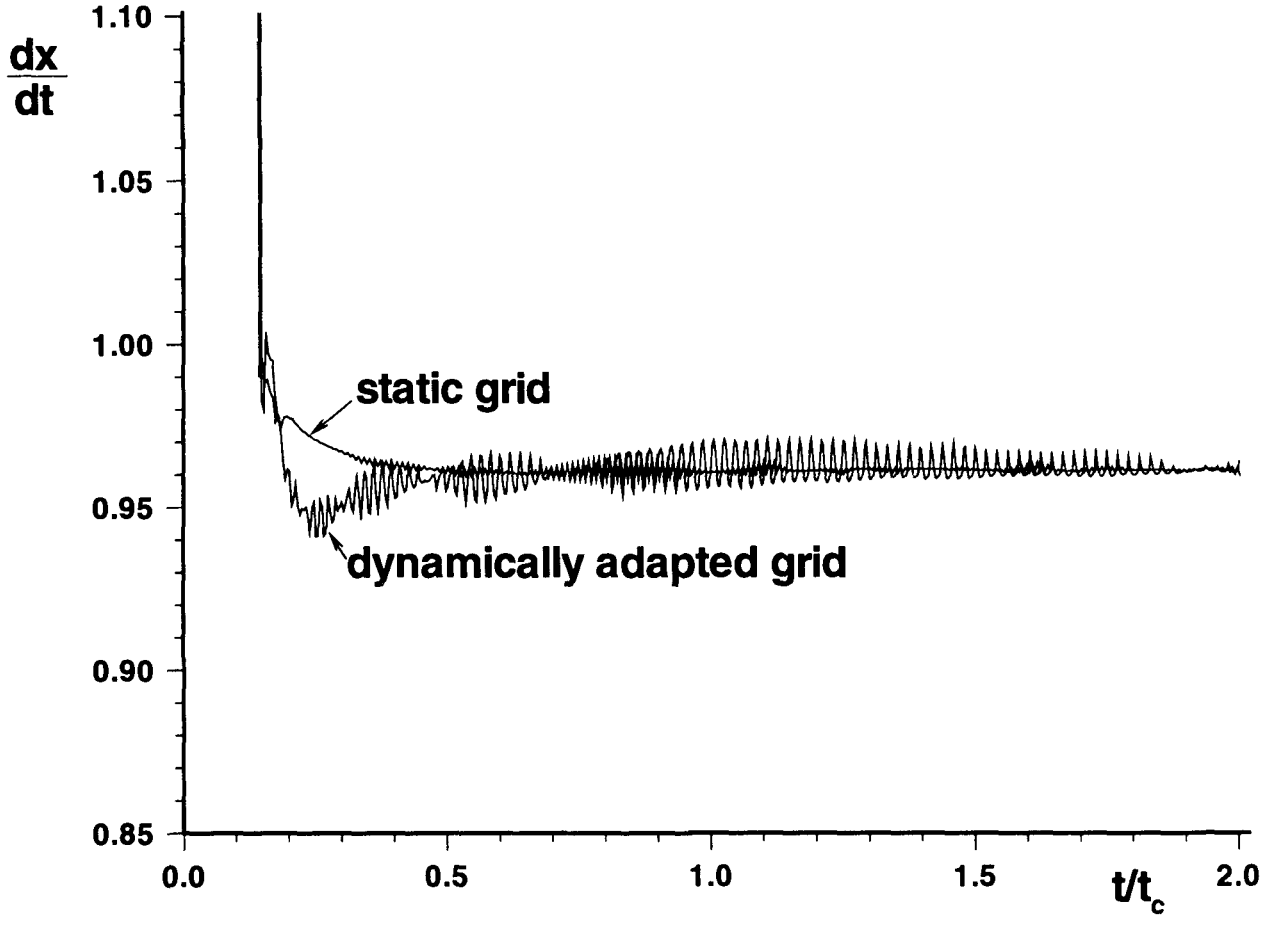

Figure 3: Shock speed versus non–dimensional time for a planar shockwave.

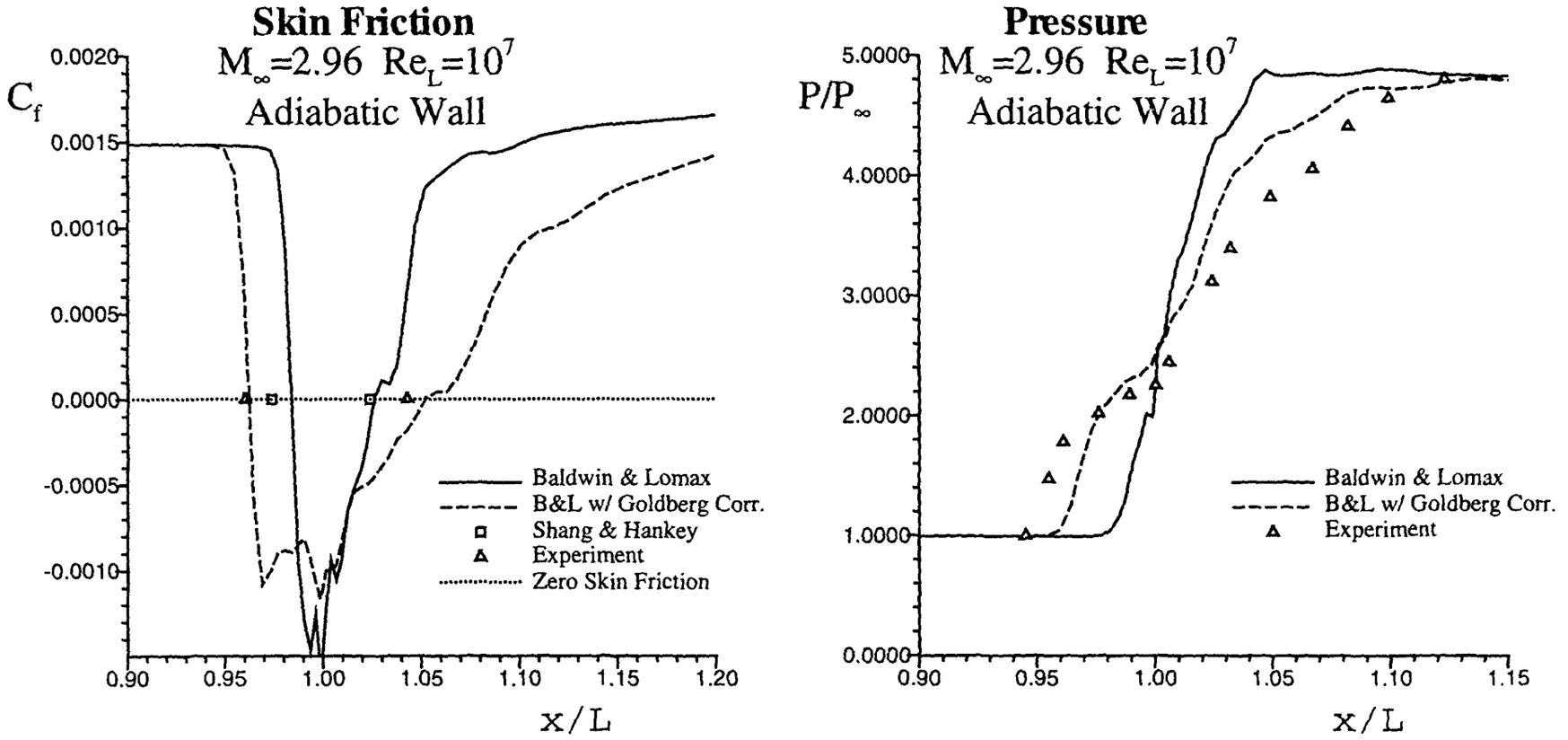

Figure 4: Skin friction and pressure plots comparing Standard B-L with B-L/Goldberg Corr. for turbulent flow over a 25° wedge.

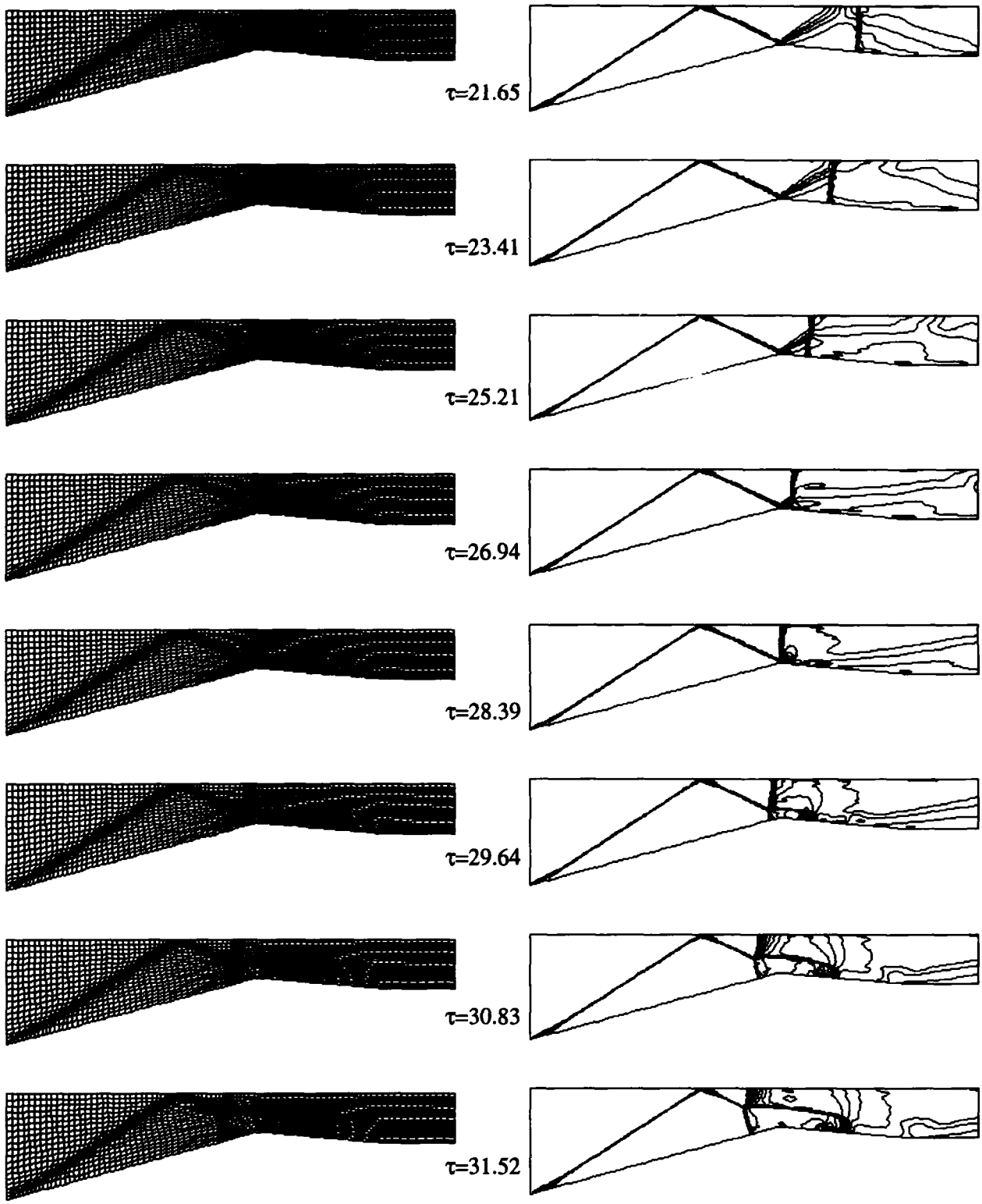

Figure 5: Series of Adapted Grid and Density Contours for Inviscid Inlet Unstart using Pb/Pinf = 24.0

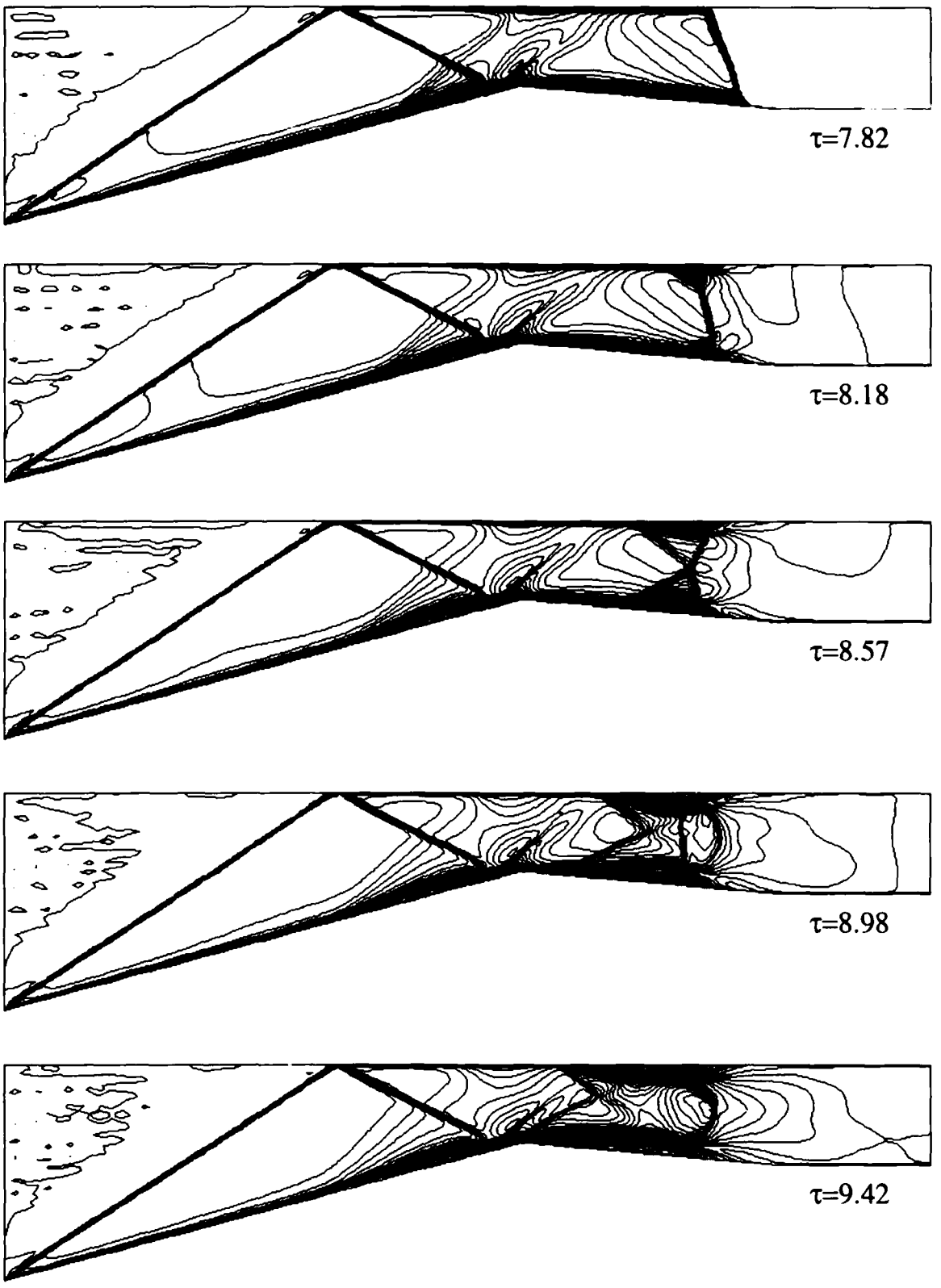

Figure 6a: Mach Contour Series for the Viscous Inlet Unstart
Pb/Pinf = 30.0

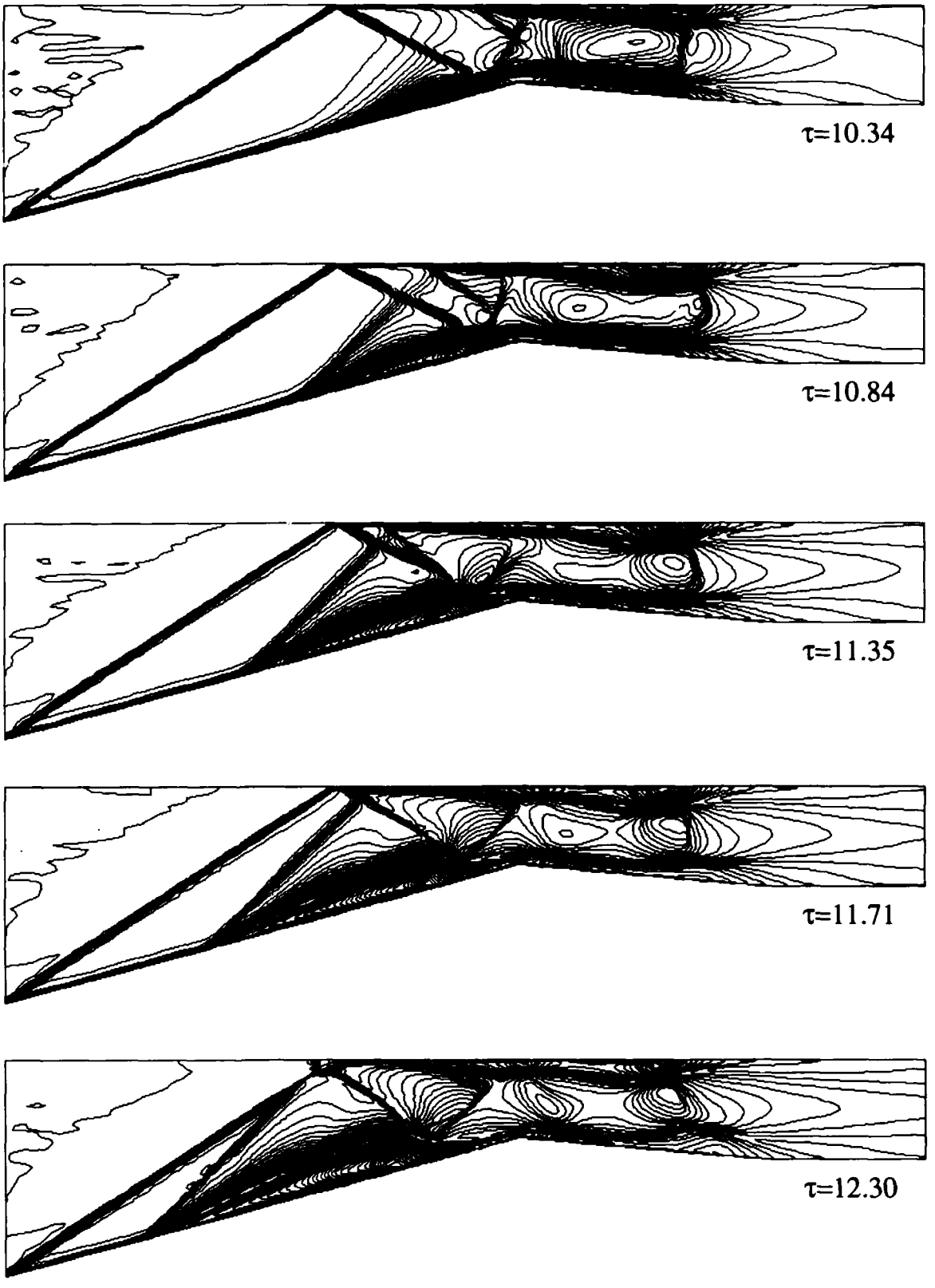

Figure 6b: Mach Contour Series for the Viscous Inlet Unstart (cont'd)
Pb/Pinf = 30.0

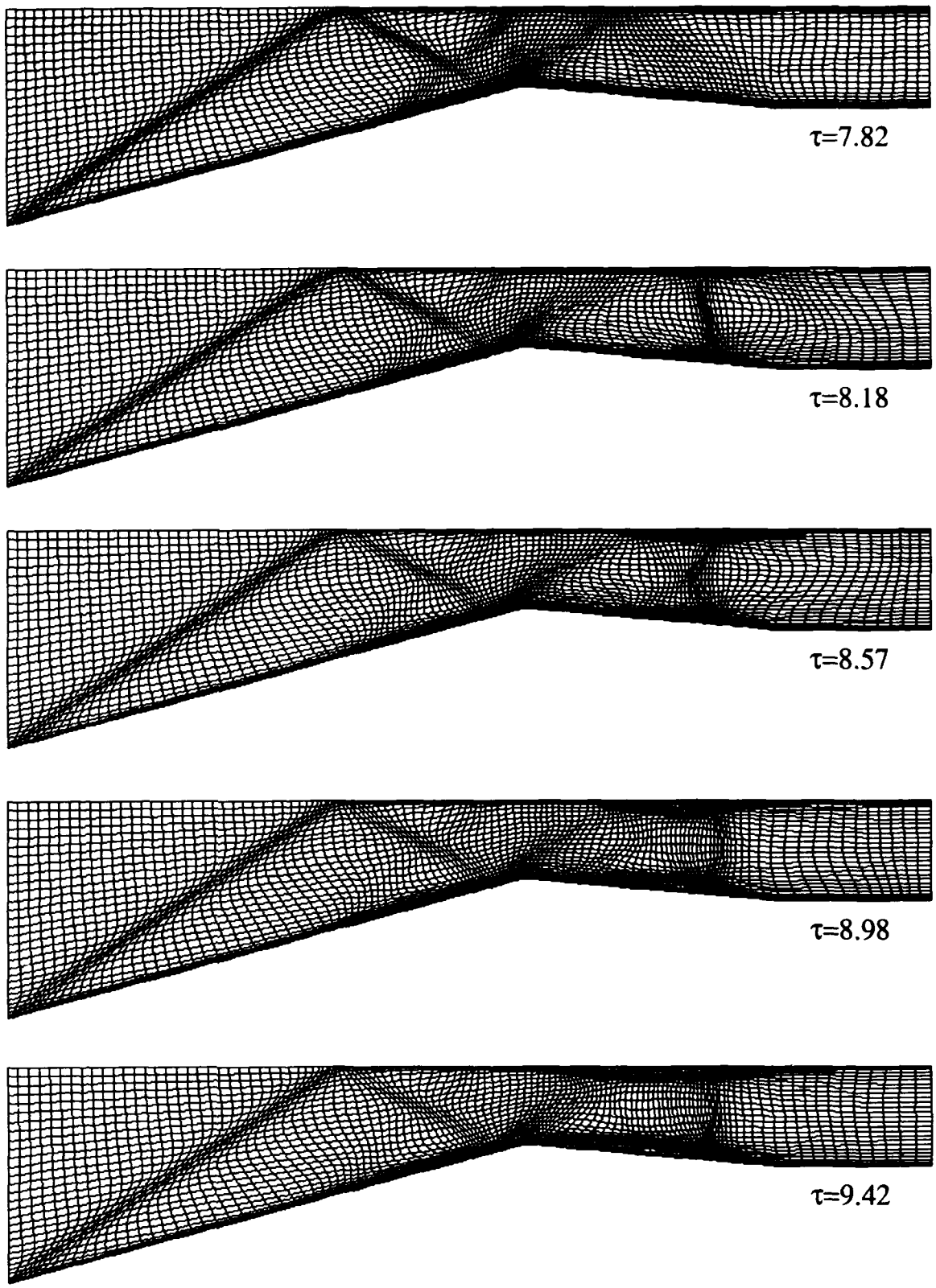

Figure 7a: Adapted Grid Series for the Viscous Inlet Unstart
(Note: every other grid line in the normal direction)

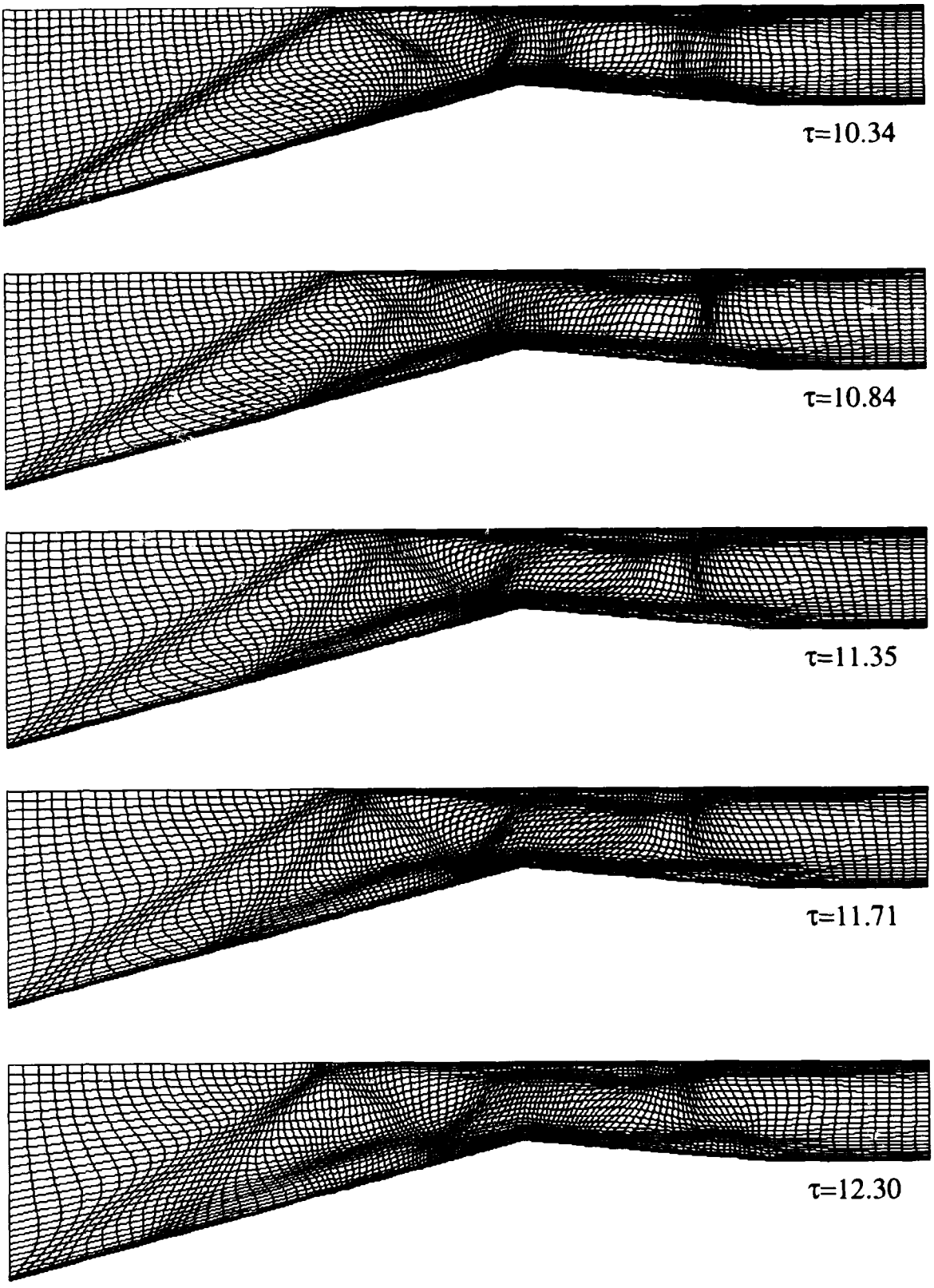

Figure 7b: Adapted Grid Series for the Viscous Inlet Unstart (cont'd)
(Note: every other grid line in the normal direction)

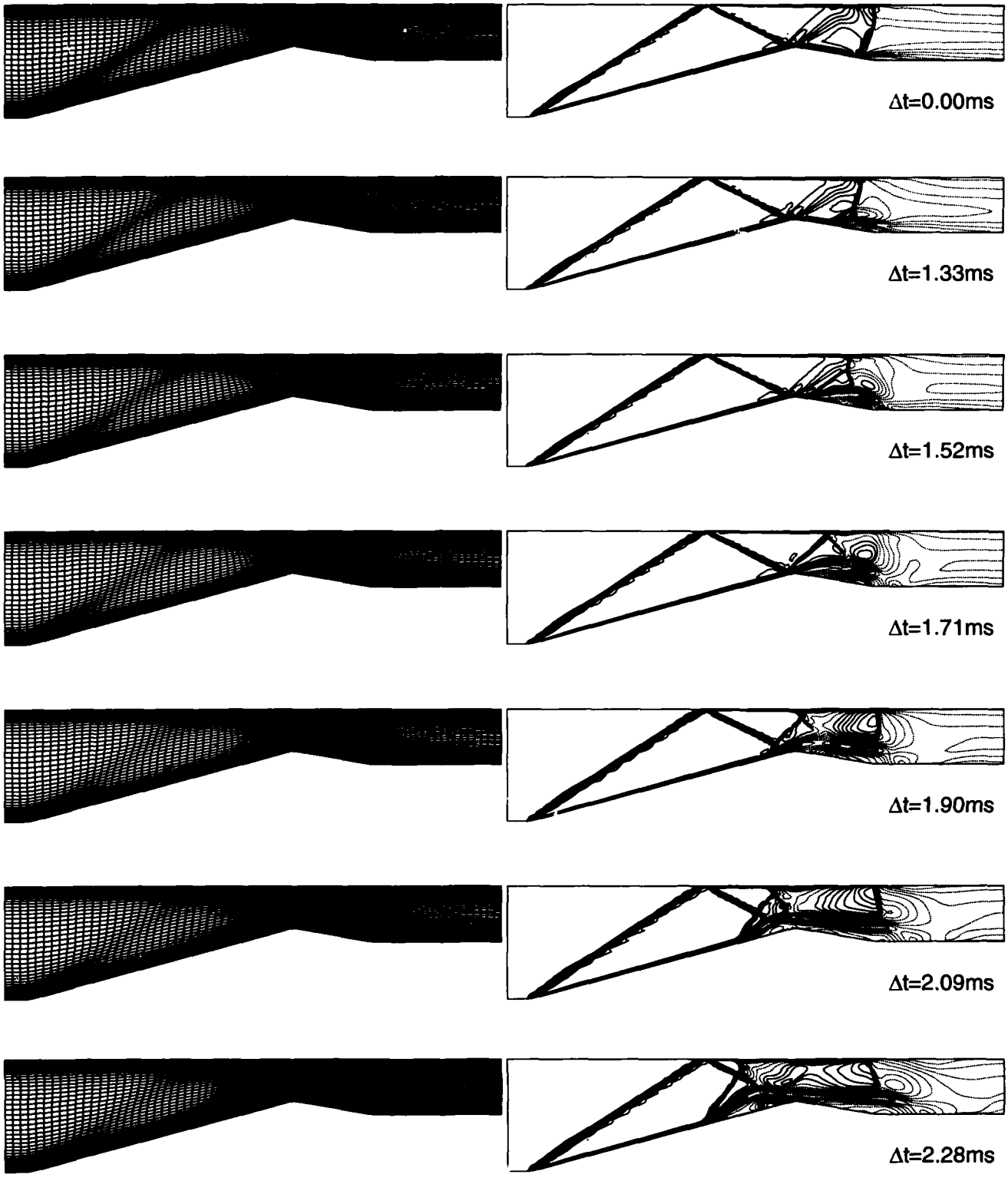

Figure 8: Adaptive Grid and Mach Contour Time–History of 2–D Turbulent Unstart. Back Pressure was increased from 17P_{inf} to 23P_{inf} starting at t=0.00ms over 1ms. ----- Supersonic ..... Subsonic

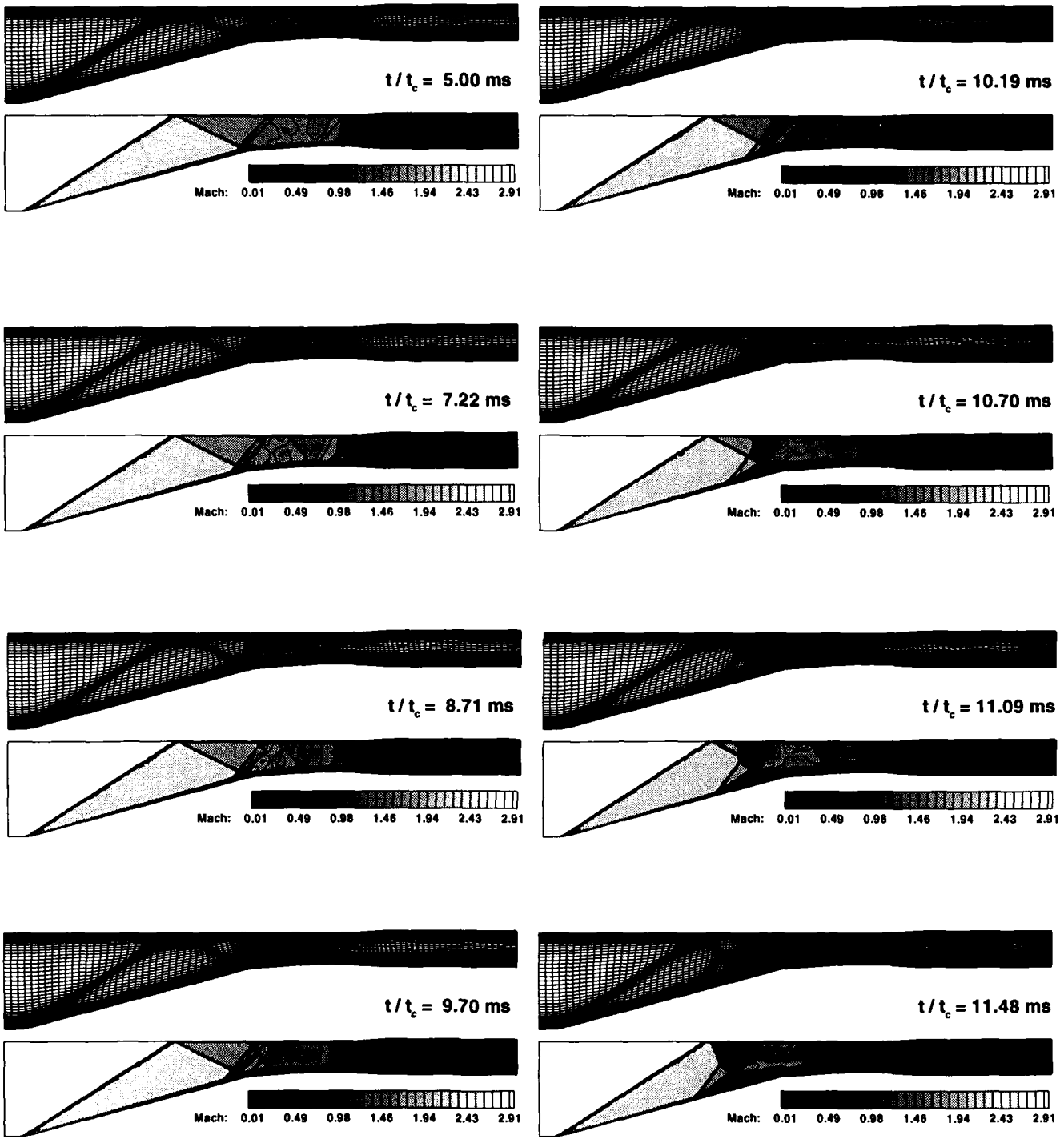

Figure 9: Grid and Mach contour series for a freestream onset angle of –1.0 degree

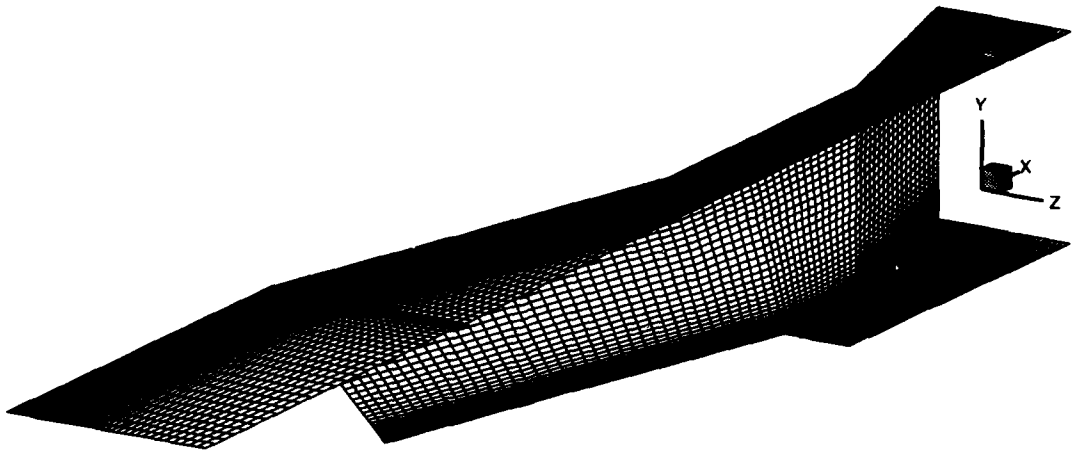

Figure 16: Initial grid for the M=10 3–D inlet of Holland.

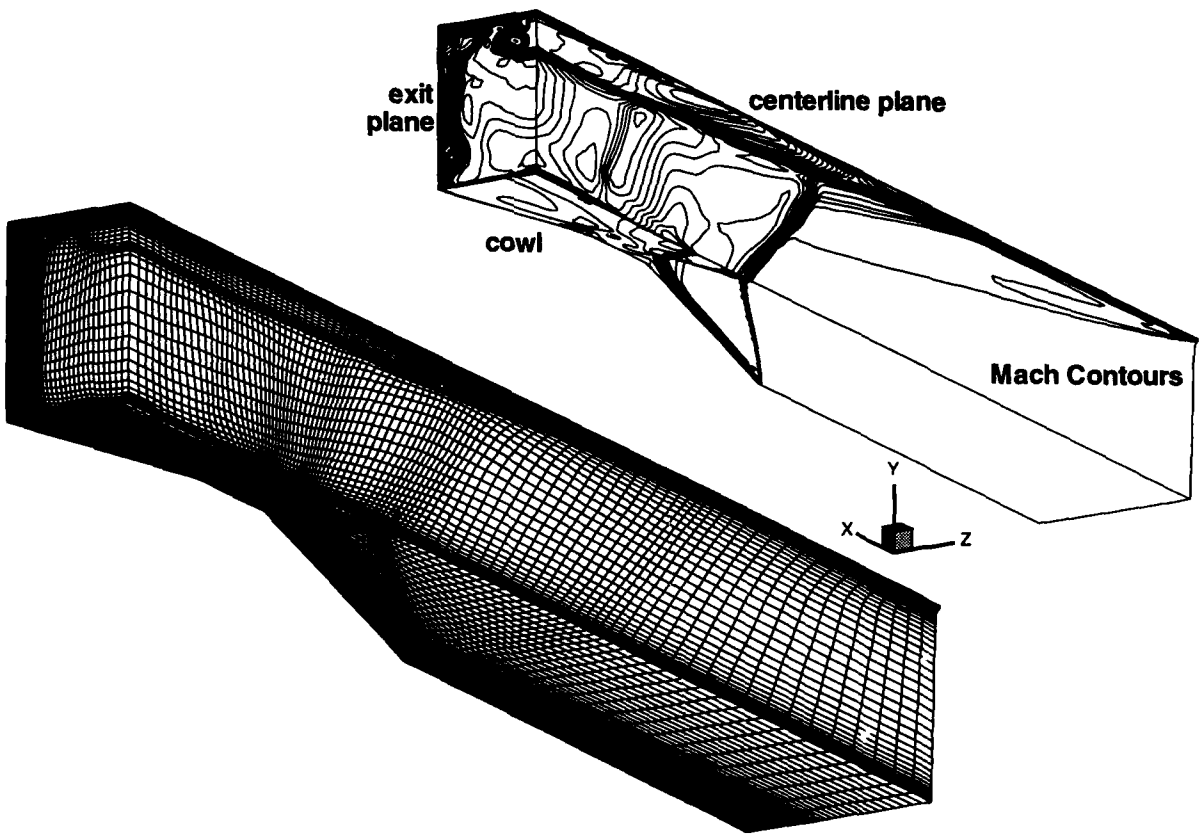

Figure 17: Orthographic projection of the grid and Mach contours in the cowl, exit and baseplate centerline planes. (z enlarged 26.7%) (Holland)

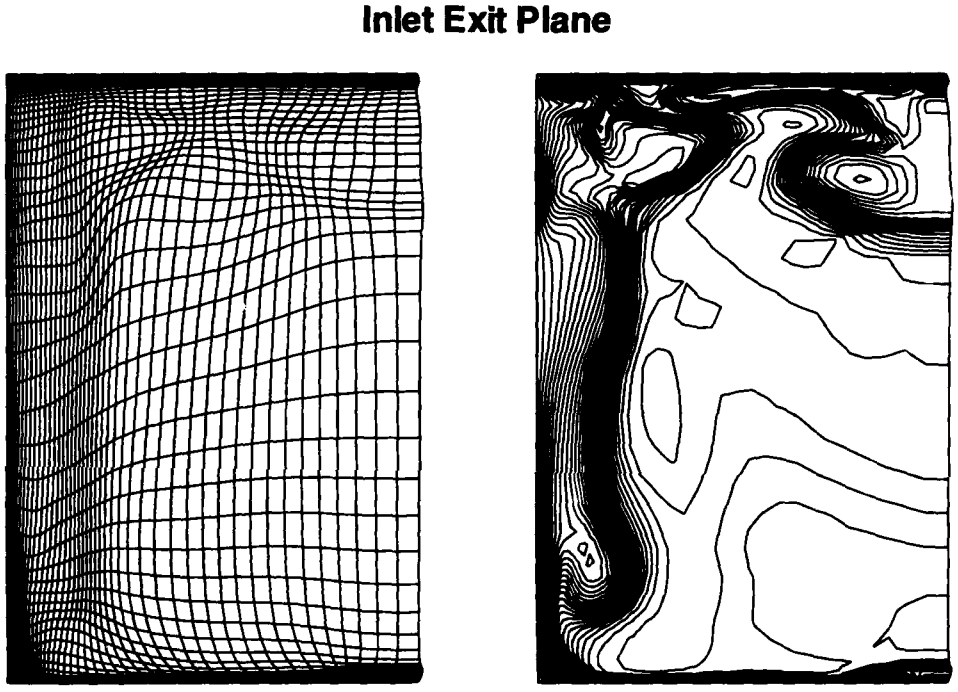

Figured 18: Adapted grid and Mach contours in the inlet exit plane. (z enlarged 267%) (Holland)

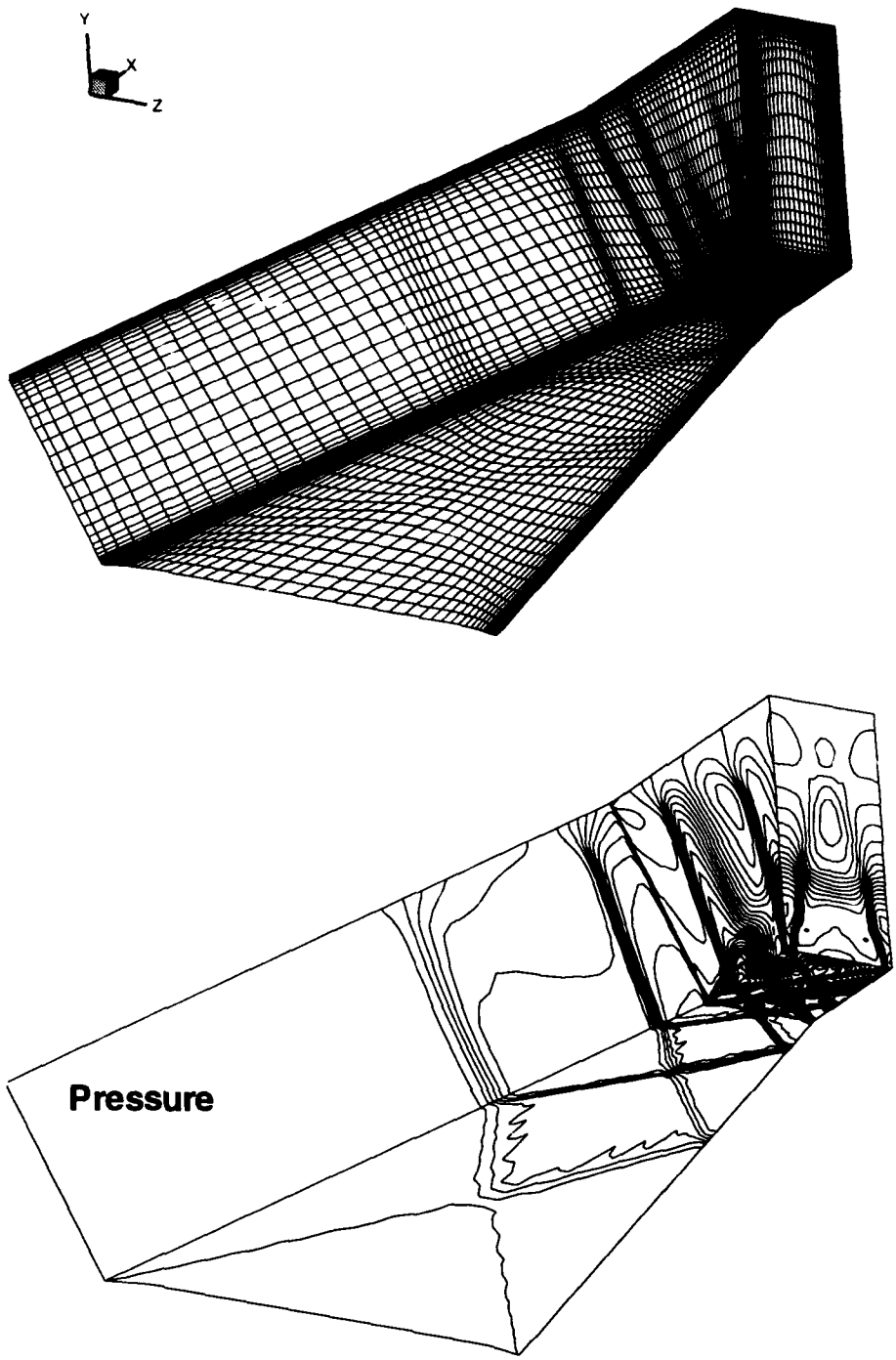

Figure 19: Adapted grid and pressure contours for the 3–D inlet of Korte, et. al..

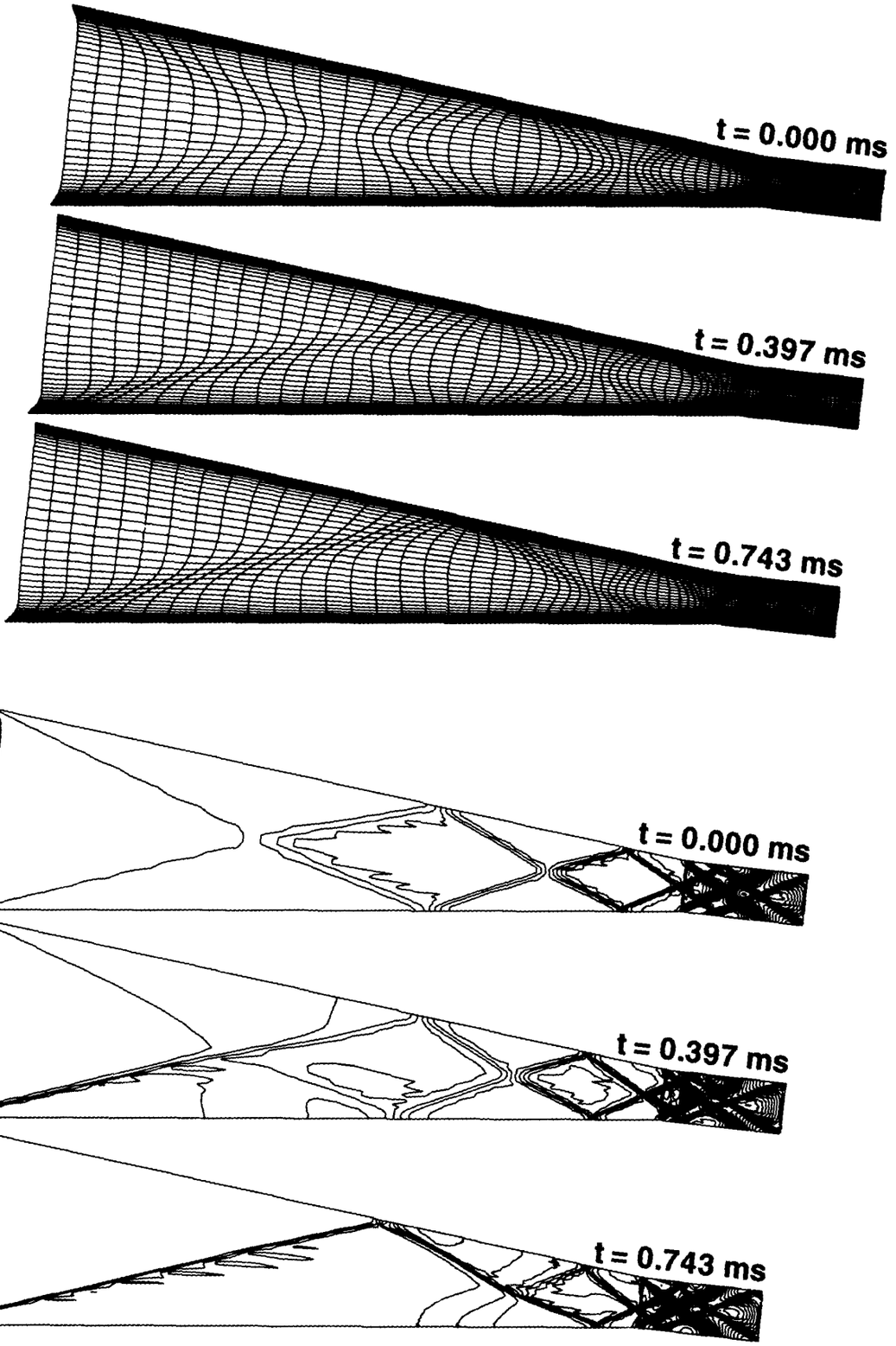

Figure 20: Series of adapted grid and pressure contours in the cowl plane for the 3–D Inlet of Korte, et.al. subject to a yaw angle of 5.5 degrees.

Boeing Commercial Airplane Group
P.O. Box 3707
Seattle, WA 98124-2207

February 21, 1994
PROP-BNB5B-JHG-L013

Dr. Leonidas M. Sakell
AFOSR/NA
110 Duncan Avenue - suite B115
Bolling AFB
Washington DC 20332

BOEING

Dear Dr. Sakell:

We want to thank you for your prompt response to our request to approve release of the NASA Contractor Report on Advanced Concept Studies to Professor Scott McRae (North Carolina State University). I also wanted to note that we have found the work of Professor McRae and his student, Rusty Benson very valuable and complementary to Boeing work in support of the High Speed Civil Transport. What we learned from the recent paper presented by Benson and McRae, **Unsteady Transients in a Supersonic Inlet Subject to Freestream Perturbations and Dynamic Attitude changes**, AIAA Paper 94 - 0581, has advanced our understanding of how an inlet responds to such disturbances by a number of months. Because these calculations are so computer intensive, we have been forced to neglect viscous effects in our in - house simulations and concentrate our work on bleed and compressor face boundary conditions. Benson and McRae pointed out that if a shock induced separation occurs in the inlet throat because of a decrease in engine demand, the disturbance will propagate forward at the *local speed of sound (much faster than* the propagation speed of the normal shock). This fact has important implications for us in design of the normal shock stability system for the HSCT.

We think the work of Benson and McRae under Air Force Grant F4960-92-J-0189 represents a great example of Technology Transfer from government supported research to industry. As you know, discussions are underway to coordinate our research with that underway for the AFOSR. We look forward to a continued productive interaction with you pertaining to unsteady flow effects associated with inlets. Keep up the good work!

Sincerely,

John H. Gerstle, Manager
HSCT Propulsion
(206)237-7571 M/S 6H-FJ

sh

cc: Professor Scott McRae
North Carolina University